

POLITECNICO DI TORINO

Master of Science in Automotive Engineering

Master's Degree Thesis

**Installation on the test bench and  
preliminary testing of a light-duty  
diesel engine for commercial  
vehicle toward EU 7 regulations**



**Academic Supervisors**  
Prof. Stefano d'Ambrosio  
Dott. Alessandro Mancarella

**Candidate**  
Fabio Napoli

Academic Year 2019-2020



# Sommario

I veicoli commerciali leggeri devono rispettare limiti su emissioni inquinanti molto restrittivi che diventeranno sempre più stringenti nel prossimo futuro. Attualmente, la verifica delle emissioni del veicolo in condizioni di guida reali tramite nuovi strumenti di misura rende l'adempimento dei limiti imposti molto più impegnativo rispetto al passato. Per questo motivo, le strategie di controllo dei motori assumono grande rilevanza ed è necessario ottimizzare il loro funzionamento in ogni condizione di utilizzo del motore, al fine di raggiungere la riduzione delle emissioni inquinanti e allo stesso tempo prestazioni adeguate. La calibrazione al banco prova è fondamentale perché permette di effettuare test sperimentali che simulano l'utilizzo reale del motore in modo da trovare il valore ottimale di ciascun parametro fondamentale.

L'attività descritta in questa tesi è il risultato del lavoro svolto presso il Dipartimento di Energia (DENERG) del Politecnico di Torino negli ultimi sette mesi. Tale attività è stata svolta nel laboratorio dei motori a combustione interna (ICEAL) dove è presente una sala prova dinamica per l'esecuzione di test sperimentali. Lo scopo è stato quello di utilizzare il motore diesel fornito da FPT per definire strategie di calibrazione indirizzate alla riduzione delle emissioni inquinanti. Durante la fase iniziale del progetto il motore è stato adattato e poi installato in cella. Infine, è stato definito un piano di test sperimentali con lo scopo di determinare il funzionamento del circuito EGR e il suo impatto sul funzionamento del motore. I risultati ottenuti consentiranno in futuro l'esecuzione di test mirati all'implementazione di strategie di controllo avanzate.

# Abstract

Light-duty commercial vehicles must comply with very restrictive limits on pollutant emissions, which will be continuously tightened over the next years. Today, the testing of vehicle emissions in real driving conditions by using new measuring instruments makes compliance with the limits set much more demanding than in the past. Therefore, the engine control strategies take on great importance, and it is necessary to optimize them over all the engine operating range to achieve the reduction of pollutant emissions as well as satisfactory performances. Calibration on the test bench is essential because by performing experimental tests that simulate the real use of the engine, it is possible to find the optimal value of each relevant parameter.

The activity described in this thesis is the result of the work at the Energy Department (DENERG) of the Politecnico di Torino in the last seven months. This activity was carried out in the Internal Combustion Engine Laboratory (ICEAL), where a dynamic test cell was used for running experimental tests. The aim was to use the diesel engine provided by FPT to investigate calibration strategies for reducing pollutant emissions. During the first phase of the project, the engine was adapted and then installed inside the test cell. Finally, a plan of several experimental tests was defined to determine the EGR circuit functioning and its impact on the engine. The results obtained will allow to run tests in the future aimed at implementing advanced control strategies.



# Contents

<b>List of Figures</b>	VIII
<b>List of Tables</b>	XII
<b>1 Diesel Conventional Combustion</b>	1
1.1 Conceptual Model of DI Diesel Combustion . . . . .	1
1.2 Fuel Spray Development . . . . .	3
1.3 Heat-Release Rate analysis . . . . .	5
1.4 Diesel fuels . . . . .	8
<b>2 Pollutant emissions in Diesel engines</b>	11
2.1 Nitrogen Oxides . . . . .	12
2.1.1 Nitric Oxide . . . . .	12
2.1.2 Nitrogen Dioxide . . . . .	14
2.1.3 NO <sub>x</sub> in Diesel Combustion . . . . .	15
2.2 Particulate Matter . . . . .	15
2.3 Unburned Hydrocarbons . . . . .	17
2.4 Carbon Monoxide . . . . .	18
2.5 Emissions Control . . . . .	18
<b>3 Experimental Setup</b>	20
3.1 Test cell and Control room . . . . .	21
3.1.1 Dynamometer . . . . .	22
3.1.2 Engine . . . . .	23
3.1.3 Cooling System . . . . .	24
3.2 Sensors for data acquisition . . . . .	24

3.2.1	Pressure sensors . . . . .	24
3.2.2	Temperature sensors . . . . .	25
3.2.3	Mass Air Flow Sensor . . . . .	25
3.2.4	Exhaust Gas Analyzers . . . . .	26
3.3	Fuel Metering System . . . . .	28
3.4	Emissions measurement equipment . . . . .	28
3.4.1	Non-Dispersive Infrared Analyzer . . . . .	29
3.4.2	Chemiluminescence Analyzer . . . . .	30
3.4.3	Flame Ionization Detector . . . . .	32
3.4.4	Paramagnetic Detector . . . . .	32
3.4.5	Particulate Analyzers . . . . .	33
<b>4</b>	<b>Results</b>	<b>35</b>
4.1	Combustion process . . . . .	40
4.1.1	In-cylinder pressure . . . . .	40
4.1.2	Net Heat-Release Rate . . . . .	42
4.1.3	Cumulative Heat-Release Rate . . . . .	43
4.1.4	Brake specific fuel consumption, Coefficient of variation and MFB50 . . . . .	44
4.2	Pollutant Emissions . . . . .	45
4.3	System parameters . . . . .	50
<b>5</b>	<b>Future developments</b>	<b>56</b>
5.1	Test plan . . . . .	56
5.2	Alternative fuels . . . . .	60
<b>6</b>	<b>Conclusions</b>	<b>63</b>
<b>A</b>	<b>List of sensors</b>	<b>65</b>
	<b>Bibliography</b>	<b>69</b>

# List of Figures

1.1	Conceptual model of DI Diesel combustion[2]. . . . .	2
1.2	Sauter Mean Diameter dependencies on injection pressure, nozzle diameter, fuel viscosity and surface tension[3]. . . . .	5
1.3	Diesel spray evolution before the combustion process[3]. . . . .	6
1.4	Heat-Release Rate and combustion phases in conventional mode[3].	7
2.1	Typical exhaust gas composition in Diesel engines[10]. . . . .	12
2.2	NO concentrations in equilibrium and kinetically controlled conditions[10]. . . . .	13
2.3	NO <sub>2</sub> concentration in different operating points[3]. . . . .	14
2.4	Main components of the Particulate Matter[3]. . . . .	16
2.5	Soot mass fraction evolution in Diesel engines[10]. . . . .	17
3.1	Typical experimental setup[13]. . . . .	20
3.2	AVL APA 100 Dynamometer[14]. . . . .	23
3.3	F1A architecture and sensors positioning. . . . .	27
3.4	AVL KMA 4000[14]. . . . .	28
3.5	Typical measuring line[19]. . . . .	29
3.6	Non-Dispersive Infrared Analyzer[20]. . . . .	30
3.7	ChemiLuminescence Detector[20]. . . . .	31
3.8	Flame Ionization Detector[20]. . . . .	32
3.9	Paramagnetic Detector[20]. . . . .	33
3.10	Opacity meter[20]. . . . .	34
3.11	Smoke meter[20]. . . . .	34

4.1	Temperature inside the intake manifold for different HP-LP combinations. $\lambda = 2.67 \pm 0.015$ . . . . .	36
4.2	Nitrogen Oxides emissions for different HP-LP combinations. $\lambda = 2.67 \pm 0.015$ . . . . .	37
4.3	Cylinder # 1 IMEP and PMEP for different HP-LP combinations. $\lambda = 2.67 \pm 0.015$ . . . . .	37
4.4	Brake specific fuel consumption for different HP-LP combinations. $\lambda = 2.67 \pm 0.015$ . . . . .	38
4.5	Net Heat-Release Rate of cylinder #1 for different HP-LP combinations. $\lambda = 2.67 \pm 0.015$ . . . . .	38
4.6	Center of combustion MFB50 for different HP-LP combinations. $\lambda = 2.67 \pm 0.015$ . . . . .	39
4.7	In-cylinder #1 pressure for different HP-LP combinations. $\lambda = 2.67 \pm 0.015$ . . . . .	40
4.8	In-cylinder #1 pressure for different HP-LP combinations. $\lambda = 2.67 \pm 0.015$ . . . . .	40
4.9	In-cylinder #1 pressure for different HP-LP combinations. $\lambda = 2.10 \pm 0.015$ . . . . .	41
4.10	In-cylinder #1 pressure for different HP-LP combinations. $\lambda = 2.10 \pm 0.015$ . . . . .	41
4.11	Net Heat-Release Rate of cylinder #1 for different HP-LP combinations. $\lambda = 2.67 \pm 0.015$ . . . . .	42
4.12	Net Heat-Release Rate of cylinder #1 for different HP-LP combinations. $\lambda = 2.10 \pm 0.015$ . . . . .	42
4.13	Net Heat-Release Rate of cylinder #1 for different HP-LP combinations. $\lambda = 2.10 \pm 0.015$ . . . . .	43
4.14	Cumulative Heat-Release Rate of cylinder #1 for different HP-LP combinations. $\lambda = 2.67 \pm 0.015$ . . . . .	43
4.15	Brake specific fuel consumption for different HP-LP combinations. $\lambda = 2.10 \pm 0.015$ . . . . .	44
4.16	Center of combustion MFB50 for different HP-LP combinations. $\lambda = 2.10 \pm 0.015$ . . . . .	44
4.17	Cylinder # 1 IMEP and PMEP for different HP-LP combinations. $\lambda = 2.10 \pm 0.015$ . . . . .	45

4.18	Carbon Monoxide emissions for different HP-LP combinations. $\lambda = 2.67 \pm 0.015$ . . . . .	45
4.19	Unburned Hydrocarbons emissions for different HP-LP combinations. $\lambda = 2.67 \pm 0.015$ . . . . .	46
4.20	Nitric Oxide emissions for different HP-LP combinations. $\lambda = 2.67 \pm 0.015$ . . . . .	46
4.21	Carbon Monoxide emissions for different HP-LP combinations. $\lambda = 2.10 \pm 0.015$ . . . . .	47
4.22	Unburned Hydrocarbons emissions for different HP-LP combinations. $\lambda = 2.10 \pm 0.015$ . . . . .	47
4.23	Nitric Oxide emissions for different HP-LP combinations. $\lambda = 2.10 \pm 0.015$ . . . . .	48
4.24	Nitrogen Oxides emissions for different HP-LP combinations. $\lambda = 2.10 \pm 0.015$ . . . . .	48
4.25	NOx vs HC trade-off for different HP-LP combinations. $\lambda = 2.67 \pm 0.015$ . . . . .	49
4.26	NOx vs HC trade-off for different HP-LP combinations. $\lambda = 2.67 \pm 0.015$ . . . . .	49
4.27	Air pressure after Inter-cooler for different HP-LP combinations. $\lambda = 2.67 \pm 0.015$ . . . . .	50
4.28	Exhaust pressure before turbocompressor for different HP-LP combinations. $\lambda = 2.67 \pm 0.015$ . . . . .	50
4.29	Pressure after HP EGR cooler for different HP-LP combinations. $\lambda = 2.67 \pm 0.015$ . . . . .	51
4.30	Temperaure after HP EGR cooler for different HP-LP combinations. $\lambda = 2.67 \pm 0.015$ . . . . .	51
4.31	Temperaure after HP EGR cooler for different HP-LP combinations. $\lambda = 2.67 \pm 0.015$ . . . . .	52
4.32	Air pressure after Inter-cooler for different HP-LP combinations. $\lambda = 2.10 \pm 0.015$ . . . . .	52
4.33	Exhaust pressure before turbocompressor for different HP-LP combinations. $\lambda = 2.10 \pm 0.015$ . . . . .	53
4.34	Pressure after HP EGR cooler for different HP-LP combinations. $\lambda = 2.10 \pm 0.015$ . . . . .	53

4.35	Temperature inside the intake manifold for different HP-LP combinations. $\lambda = 2.10 \pm 0.015$ . . . . .	54
4.36	Temperaure after HP EGR cooler for different HP-LP combinations. $\lambda = 2.10 \pm 0.015$ . . . . .	54
4.37	Temperaure after HP EGR cooler for different HP-LP combinations. $\lambda = 2.10 \pm 0.015$ . . . . .	55
5.1	Definition of test speeds[22]. . . . .	58
5.2	Definition of test reference speed[22]. . . . .	59
5.3	Engine map. . . . .	60

# List of Tables

1.1	EN 590 standard for automotive diesel fuels[8]. . . . .	10
3.1	Engine parameters. . . . .	23
3.2	Kistler pressure sensors characteristics[17]. . . . .	25
3.3	Thermocouples characteristics[18, p. 4]. . . . .	25
4.1	Values of the main test variables. O=Open and C=Closed. . . . .	35
4.2	Test plan. . . . .	36
5.1	Vehicle dataset. . . . .	56
5.2	Test plan. . . . .	56
5.3	WHSC[22]. . . . .	59
5.4	Technical characteristics of HVO and B7 fuels. . . . .	61
A.1	List of sensors of the experimental setup. . . . .	66
A.2	List of sensors of the experimental setup. . . . .	67
A.3	List of sensors of the experimental setup. . . . .	68



# Nomenclature

## Acronyms

**CN** Cetane Number

**EMF** Electromotive force

**ATS** After-treatment system

**BMEP** brake mean effective pressure

**BSFC** Brake specific fuel consumption

**CEN** European Committee for Standardization

**CLD** Chemiluminescence Detector

**DOC** Diesel oxidation catalyst

**DPF** Diesel particulate filter

**ECU** Engine control unit

**EGR** Exhaust gas recirculation

**ESC** European Stationary Cycle

**FAME** Fatty Acid Methyl Ester

**FID** Flame Ionization Detector

**FPT** Fiat Powertrain Technologies

**FSN** Filter Smoke Number

**GHG** Green House Gas

**GTR** Global Technical Regulation

**HP-EGR** High Pressure EGR

**HVO** Hydrotreated Vegetable Oil

**ICEAL** Internal combustion engine advanced laboratory

**ISO** International Organization for Standardization

**LP-EGR** Low Pressure EGR

**NDIR** Non-Dispersive Infrared Analyzer

**PAH** Polycyclic Aromatic Hydrocarbons

**PM** Particulate matter

**SCR** selective catalytic reduction

**SMD** Sauter mean diameter

**SOC** Start of Combustion

**SOF** Soluble organic fraction

**SOI** Start of Injection

**UNECE** United Nations Economic Commission for Europe

**UUT** Unit Under Test

**VGT** Variable geometry turbocharger

**WHSC** World Harmonized Steady State Cycle

### **Symbols**

$\tau$  Transmittance

$\gamma$  Specific heat ratio

$\lambda$  Relative air to fuel ratio

$\phi$	Equivalence ratio
$\mathbf{A}/\mathbf{F}$	Air to fuel ratio
$\mathbf{h}_f$	Specific enthalpy of the fuel
$\mathbf{I}$	Light intensity
$\mathbf{m}_f$	Mass of the fuel
$\mathbf{p}$	Cylinder pressure
$\mathbf{Q}_{ch}$	Fuel chemical energy release or gross heat release
$\mathbf{Q}_{ht}$	Heat transfer to the wall
$\mathbf{Q}$	Heat transfer
$\mathbf{T}$	Temperature
$\mathbf{U}$	Internal energy
$\mathbf{V}$	Cylinder volume



# Chapter 1

# Diesel Conventional Combustion

Numerical models for a quantitative investigation of the diesel combustion process are today widespread in the automotive field. However, a quantitative analysis is only possible if the features of the phenomenon under studying are already known. For this reason, a comprehensive qualitative model of the combustion process is essential and will be the subject of the following sections.

## 1.1 Conceptual Model of DI Diesel Combustion

The model described in this section was the result of a massive amount of investigations carried out mainly at the Sandia National Laboratories by J. Dec and his team. They published it in the late 1990s and, in the following years became a milestone of the internal combustion engine literature since it provides a reliable and accurate conceptual model of the diesel combustion process[1]. The experimental activity was based on the use of innovative optical techniques. For this reason, it was realized by using a single-cylinder DI engine suitably modified for the installation of the optical instrumentation[1]. It is essential to state that the model does not take into consideration wall interactions and swirl motion[1].

The process begins with the fuel injection and the jet development. The first breakthrough of the model, as compared with the previous one, refers to the relative penetration inside the combustion chamber of the liquid and vapor phases. When

the liquid core reaches the maximum penetration, the vapor mixture formed in the meanwhile penetrates to a greater extent[1]. Liquid fuel is injected into the combustion chamber through the injector nozzle just before the desired start of the combustion, generally toward the end of the compression stroke. The fuel at a relatively low temperature of about 350 K penetrates a high-pressure - high-temperature environment, mixes with warm air (950 K) and starts vaporizing[2]. Then, a mixture of gaseous fuel and air forms around the liquid core, beginning from the side of the jet[1]. At a temperature of 750 K the initial chemical reactions typical of the breakdown of the fuel start releasing additional heat until, at approximately 850 K, the oxidation reactions become increasingly faster[2].

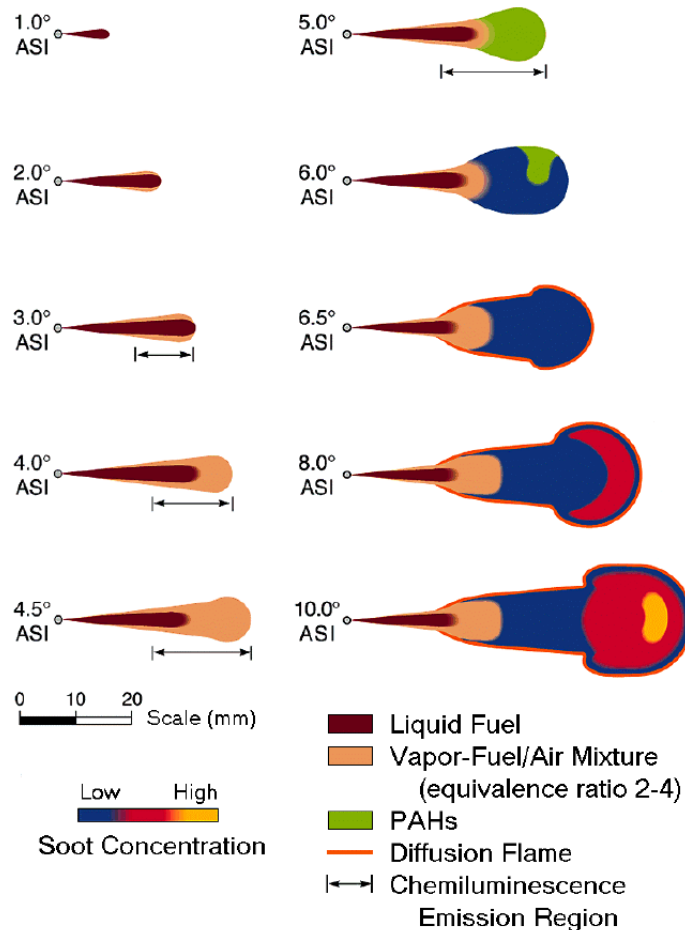


Figure 1.1: Conceptual model of DI Diesel combustion[2].

Immediately after auto-ignition, the premixed burning phase begins, and it results in partial oxidation of the fuel and the release of the relative chemical energy. At the end of this phase, the local conditions can be well described by a temperature of 1600 K in an environment rich of fuel fragments (Polycyclic Aromatic Hydrocarbons - PAH), CO, CO<sub>2</sub>, and water vapor[2]. Toward the end of the premixed burning phase, a thin diffusion layer starts forming in the surroundings of the jet until the mixing controlled phase entirely controls the combustion process. This last stage occurs in a very thin reaction zone, which is essentially the interface between the jet and region of the chamber not yet involved in the process[1]. Therefore, the fuel fragments coming from inside of the jet react with the oxygen coming from outside. The chemical energy will be released as heat, and the highest temperature of 2500 K was reached quickly[2].

The model just outlined is a synthetic explanation of the combustion process that also gives significant insights on soot and NO<sub>x</sub> formation. Soot forms during the premixed burning[1]. This phase takes place under fuel-rich conditions and its products, mainly PAH, reacts together, forming soot particles that then grows traveling towards the diffusion flame where they can be eventually oxidized[1]. NO<sub>x</sub> formation depends on oxygen concentration and temperature that must be high enough to enhance chemical reactions to an appreciable rate. For these reasons, considering the model just highlighted, it is possible to state that NO<sub>x</sub> formation does not occur during premixed burning because of the high equivalence ratio and low temperature[1]. On the contrary, NO<sub>x</sub> formation happens to a more significant extent in the diffusion flame zone, where local conditions are favourable[1]. Nevertheless, although the premixed combustion produces no significant amounts of NO<sub>x</sub>, the more intense is this phase of the combustion, the higher will be the temperature which in turn activates the NO<sub>x</sub> chemical reactions.

## **1.2 Fuel Spray Development**

In DI diesel engines, the mixture formation takes place in the combustion chamber, and it cannot be completely decoupled from the combustion process. As a consequence, spray development has a remarkable impact on the combustion process with implications in terms of fuel consumption, emissions, and noise. Its main features are the atomization, the penetration, and the arrangement in its final structure[3].

Atomization of the liquid fuel means the breakup of the fuel into small droplets. The main characteristic of the atomization is its two stage nature: the primary breakup of the liquid fuel into ligaments and droplets occurs near the nozzle and then, relatively far from it, the secondary breakup completes the atomization of droplets into smaller ones[4]. «The primary breakup of liquid jets at the nozzle exit can be caused by a combination of three mechanisms: turbulence within the liquid phase, implosion of cavitation bubbles and aerodynamic forces acting on the liquid jet»[4, p. 131]. They have different characteristics, but their effect on the liquid jet is almost the same: to disrupt the fuel stream creating increasingly smaller components. The mechanisms just introduced do not take place separately during the spray atomization[4]. Each of them interacts with the other, and the final result is a different atomization regime in which each mechanism gives its contribution[4]. Four different atomization regimes have been classified depending on the breakup length and the diameter of the final droplets[4]. In diesel engines with high injection pressure system, the one of interest is the atomization regime[4]. Secondary breakup, instead, is only related to the aerodynamics interactions between droplets and gas. Also in this case, separate mechanisms lead to different results depending on the atomization regime. However, even if all of them may be present in an operating engine, the most important is the catastrophic regime, which typically occurs near the nozzle[4]. To determine the atomization results, measures of the droplet size distributions and diameter are needed. From the previous discussion, it is clear that the atomization of the fluid results in a large number of small particles with different diameters in the order of 10  $\mu\text{m}$ [3]. Since it is impracticable to look for a direct measure of each small droplet, this kind of investigation is conducted using a statistical approach. In particular, the Sauter Mean Diameter is used. It is defined as

$$D_{SM} = \frac{\int D_d^3 dn}{\int D_d^2 dn} \quad (1.1)$$

and, by definition, « it is the diameter of a droplet that has the same volume to surface area ratio as that of the total distribution »[3, p. 560]. So, the goal of the atomization process is to minimize the SMD, and considering the SMD's trends in the Fig. 1.2, it is possible by using small nozzle diameter, high injection pressure, and fuel with low viscosity and surface tension[3].

Fuel injection and then spray formation take place progressively. The droplets

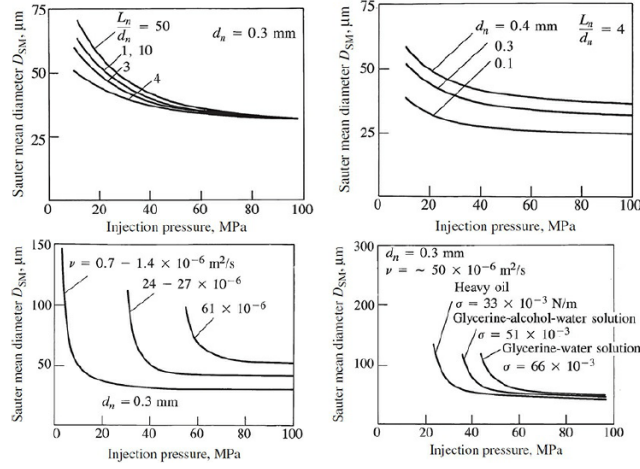


Figure 1.2: Sauter Mean Diameter dependencies on injection pressure, nozzle diameter, fuel viscosity and surface tension[3].

injected first, interact with the air, and moves it forward[3]. The droplets that are injected in a second step encounter less aerodynamic resistance and then travel a longer distance from the injector tip[3]. The droplets on the spray axis have a higher velocity than the ones on the boundary because of the higher kinetic energy[3]. This determines the spray structure, as represented in Fig. 1.3. The cone angle and the penetration are the key parameters to investigate the evolution of the spray inside the combustion chamber. The latter is crucial since overpenetration results in HC and PM emissions while under penetration in poor air utilization[3]. Penetration reduces with smaller droplets diameter[5]. Nevertheless, higher injection pressures, although they enhance atomization, generally result in higher penetration[5].

### 1.3 Heat-Release Rate analysis

The combustion phases are identified using the heat-release rate (HRR), as shown in Fig. 1.4. It is a measure of the chemical energy released by burning the fuel[3]. In order to obtain this kind of result, several methods are today available. The simplest and most used for preliminary investigations is the single zone heat-release model. It is based on the first law of thermodynamics for an open system, assuming pressure and temperature uniform inside the chamber, and allows to compute the heat-release rate by merely measuring the pressure inside the combustion chamber.

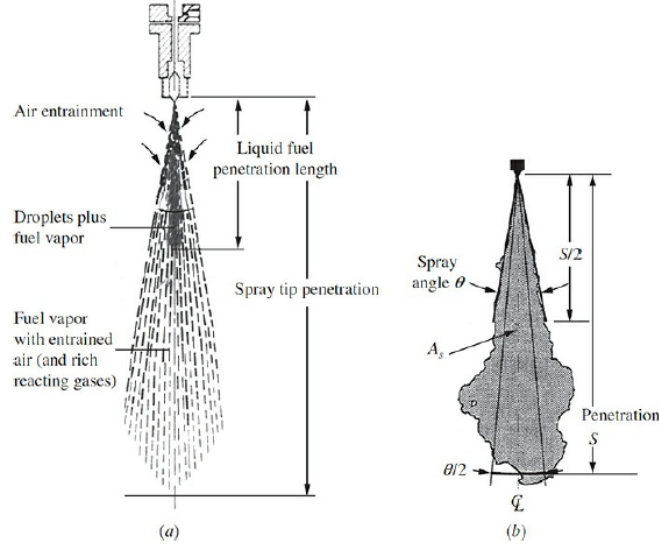


Figure 1.3: Diesel spray evolution before the combustion process[3].

The last operation, despite all the critical operational issues, can be accomplished by installing a pressure sensor inside the cylinder, as it will be explained in the following chapters. The analytical expression of the single zone model is

$$\frac{dQ}{dt} - pdV + m_f h_f = \frac{dU}{dt} \quad (1.2)$$

$$\frac{dQ_n}{dt} = \frac{dQ_{ch}}{dt} - \frac{dQ_{ht}}{dt} = pdV + \frac{dU}{dt} \quad (1.3)$$

$$\frac{dQ_n}{dt} = \frac{\gamma}{\gamma - 1} p \frac{dV}{dt} + \frac{1}{\gamma - 1} V \frac{dp}{dt} \quad (1.4)$$

where  $Q_n$  is the net heat-release rate,  $Q_{ch}$  is the gross heat-release rate, and  $Q_{ht}$  is the heat transfer to the wall. Four different phases characterize the diesel combustion process[3]:

- **Ignition delay**

It is the time interval between the Start of Injection (SOI) and the Start of Combustion (SOC), during which the fuel is injected in the combustion chamber, it atomizes, then vaporized, and eventually mixes with air to form an ignitable mixture. SOC is generally defined as the time instant at which the HRR becomes higher than zero. This phase depends on physical phenomena,

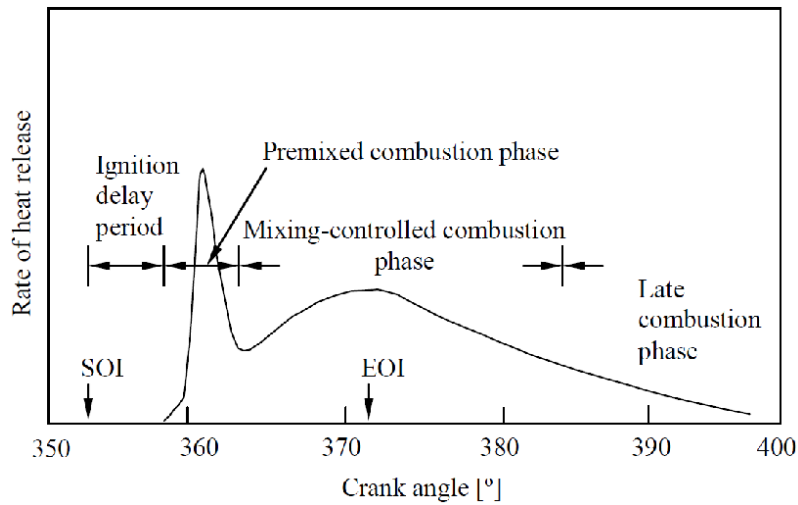


Figure 1.4: Heat-Release Rate and combustion phases in conventional mode[3].

such as atomization, vaporization, and mixing, and chemical phenomena that are taken into account by the cetane number[3].

- **Premixed combustion phase**

The premixed combustion phase refers to the combustion of only that portion of fuel accumulated during the delay period. During this phase, it is released roughly the 15% of the chemical energy of the fuel. Nevertheless, it has a substantial impact on efficiency, noise, and emissions.

- **Mixing controlled phase**

After the premixed phase, ideally, all the fuel injected during the delay period has been burned. This phase is defined as mixing-controlled because the combustion of the fuel injected subsequently the premixed phase depends on the mixing rate between fuel and air. This means that the mixing rate and the burning rate are strictly dependent. Almost all the chemical energy of the fuel is released, and temperature higher than 2500 K is reached.

- **Late combustion phase**

During the last stage, the injection of the fuel is usually ended, unless non-conventional injection strategies are exploited. All the fuel not directly involved in the main combustion process is eventually burned at a considerably lower rate.

## 1.4 Diesel fuels

Diesel fuels are the products of crude oil distillation[6]. They can be employed in different applications such as automotive, aviation, or marine engines, depending on specific characteristics. For this reason, in Europe, automotive diesel fuels are regulated by law through standards defined by the European Committee for Standardization (CEN). Above all, a first analysis of the fuel should regard the chemical composition, since a vast number of different hydrocarbons made up typical diesel fuels. Each of these compounds has a proper chemical structure, depending on the bonds and the arrangement between the atoms, which eventually affects the property of the fuel itself. The main types of hydrocarbons in automotive fuels are:

- **Aliphatic**

They can be further divided into alkanes ( $C_nH_{2n+2}$ ), alkenes ( $C_nH_{2n}$ ) and alkynes ( $C_nH_{2n-2}$ ), depending on carbon-carbon bond that is single in case of alkanes or multiple for alkenes and alkynes. They have an open chain structure which can be straight or branched.

- **Alicyclic**

Alicyclic hydrocarbons are aliphatics with a cyclic structure. In fact, the group of cycloalkanes or naphthenes ( $C_nH_{2n}$ ) is defined by the same formula as alkenes. However, they do not show double bonds but rather a ring-shaped structure[7].

- **Aromatics**

They are organic compounds characterized by a ring-shaped planar structure with additional internal bonds[7]. This involves a very low reactivity of these molecules since high energy is required to break the bonds. In diesel fuels, specific mention should be made to PAH. As for aromatics, they have a ring structure but show «two carbon atoms shared between more than one ring»[7, p. 264].

The main properties of diesel fuel are shown in Tab. 1.1. The limit values and the testing procedures are those prescribed by the CEN through the standard EN 590[8], which has been introduced in 1990 and then updated continuously over the past years. A brief description of the properties follows:

- **Cetane Number - CN**

The cetane number refers to the ignition quality of diesel fuel[3]. It is strictly related to the ignition delay between the injection of the fuel and the start of combustion. As it is known, the ignition delay is affected both by physical and chemical processes, so it is beneficial to understand what is the impact of the different phenomena occurring before the ignition. The cetane number expresses the relevance of the chemical processes, which lead to spontaneous oxidation of hydrocarbons. It is measured by comparing the ignition delay of the under-test fuel with a blend of two reference fuels: the cetane( $C_{16}H_{34}$ , CN=100) and the heptamethyl-nonane( $C_{16}H_{34}$ , CN=15). The cetane number depends on the percentage of cetane in the reference blend having the same ignition delay of the testing fuel[6]. Alkanes usually increase the cetane number, while aromatics components can have a detrimental effect on the ignition quality, due to their chemical structure[6].

- **Flash Point**

The flashpoint is the lowest temperature at which the fuel vapors produced by the liquid phase can be ignited if there are favourable conditions, namely air and a spark[3]. Generally, this property does not represent an issue in an operating diesel engine, but rather it is a risk during transport and storage of the fuel[9].

- **Carbon residue**

The carbon residue provides an index of the fuel's tendency to forming carbon deposits as a result of heat transfer[6].

- **Viscosity**

Viscosity is a measure of the fluid's internal resistance to flow[9]. For this reason, it has a substantial impact on the injection system primarily. Too high viscosity fluid may need oversized components such as injection pump or pipes[9]. On the contrary, when viscosity is very low, fuel leakages take place along the injection system and eventually result in efficiency losses[9]. Another effect of the viscosity is linked to the mixture preparation and specifically to the spray development after the injection inside the combustion chamber. Too high viscosity results in poor atomization, over penetration of the fuel, and eventually in performance losses[3]. Nevertheless, even if for opposite reasons,

very low viscosity will result in poor combustion quality since the fuel does not penetrate sufficiently[6].

- **Distillation**

As it has already said, diesel fuels are made up of several hydrocarbon compounds. As a consequence, there is no single boiling temperature but rather a boiling range. The lower limit is linked to the high volatile components: a high percentage of them result in improved cold starting ability, but it could have a negative impact on CN and lubricant properties[9]. On the contrary, the upper limit or final boiling point should not be too high to avoid soot production and nozzle coking[9].

- **PAH content**

PAH are the primary source of soot in a diesel engine[3]. For this reason, their content in diesel fuel should be limited to avoid too high engine-out soot emissions.

Table 1.1: EN 590 standard for automotive diesel fuels[8].

Property	Unit	Limits	
		Min	Max
Cetane Number		51.0	
Flash Point	$^{\circ}C$	above 55.0	
Carbon residue	$\%(m/m)$		0.30
Viscosity	$mm^2/s$	2.000	4.500
Distillation			
$\%(V/V)$ recovered at $250^{\circ}C$	$\%(V/V)$		<65
$\%(V/V)$ recovered at $350^{\circ}C$	$\%(V/V)$	85	
95 $\%(V/V)$ recovered at	$^{\circ}C$		360
PAH content	$\%(m/m)$		8.0

## Chapter 2

# Pollutant emissions in Diesel engines

Pollutant emissions have become, over the years, a primary concern in vehicles powered by internal combustion engines. They are the result of a non-ideal combustion process, but their impact on engine efficiency is minimal. Nevertheless, they are a serious issue in terms of both human health and environmental pollution. The most important pollutants regulated by law are

- Nitrogen Oxides
- Particulate Matter
- Unburned Hydrocarbons
- Carbon Monoxide

One of the primary goals of engine calibration activity is to find the optimal value for each engine parameters so that it would be possible to implement the best trade-off strategy for pollutant emissions reduction. For these reasons, it is crucial to understand what are the formation mechanisms of each pollutant species.

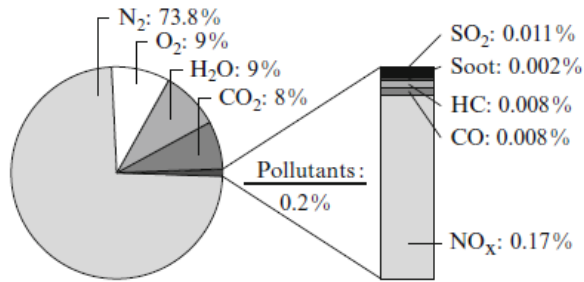


Figure 2.1: Typical exhaust gas composition in Diesel engines[10].

## 2.1 Nitrogen Oxides

Nitrogen oxides are chemical compounds of nitrogen and oxygen. In ICEs, they include nitric oxide (NO), nitrogen dioxide (NO<sub>2</sub>), and negligible traces of nitrous oxide (N<sub>2</sub>O)[3]. The relative concentrations in engine-out emissions depend on the engine type.

### 2.1.1 Nitric Oxide

NO formation mechanisms are the following[10]:

- Thermal
- Prompt
- Fuel NO
- Nitrous Oxide

NO thermal mechanism refers to the reaction involving the atmospheric nitrogen, and it was introduced by Zeldovich that identified the following reactions as the main responsible for the NO formation[3]:



The rate constant of a chemical reaction is a crucial parameter to understand the speed at which the reaction takes place. A low rate constant means the reaction will

complete after a long time. Since in the internal combustion engine, the conditions inside the chamber change continuously over a short time, if the rate constant is too low, then the reaction will never complete and there will not be an appreciable amount of its products. For these reasons, reaction 2.1 is defined as the rate limiting step of the entire formation mechanism because of the lowest reaction rate that, in turn, depends on the activation energy that is very high due to the strong nitrogen bonds[10]. Reaction 2.1 becomes relevant only at high temperatures. Furthermore, the final concentrations of the products are limited by the conditions inside the chamber, namely the sudden decrease of temperature during the process. These reactions are said to be kinetically controlled since the chemical equilibrium cannot be reached[10]. Moreover, the final concentrations of the products are higher in comparison to the ones of chemical equilibrium, as can be seen in Fig. 2.2.

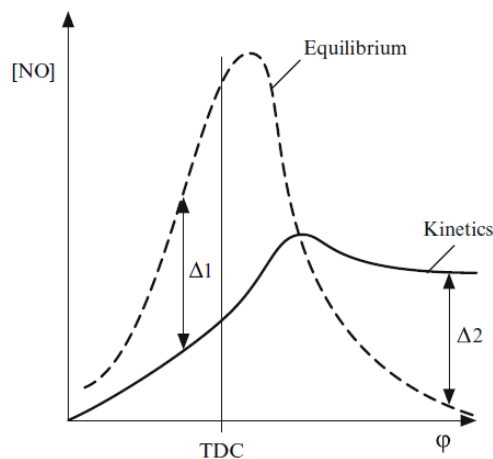


Figure 2.2: NO concentrations in equilibrium and kinetically controlled conditions[10].

No prompt mechanism was proposed by Fenimore, and it is regulated by the following reactions[10]



The distinctive characteristic of the mechanism is that it takes place only in the flame front in a relatively rich environment, where the nitrogen reacts with hydrocarbon radicals[10]. As a consequence, the formation rate of reaction 2.4 is limited by the availability of radical, that depends on the oxidation of fuel, and is inevitably very difficult to be estimated[10]. Unlike the thermal mechanism, the

prompt reaction shows a lower rate constant and activation energy, and then it must be considered only in low-temperature conditions[10].

The remaining two formation mechanisms become relevant in certain conditions; otherwise, they give a minimal contribution to the final NO<sub>x</sub> emission in diesel engines. N<sub>2</sub>O mechanism occurs only in lean, low temperature, and high-pressure environments[10]. Fuel Nitrogen mechanism refers to the reaction of the nitrogen bound in the fuel. Modern diesel fuel does not contain a significant amount of nitrogen, but it could happen that in low-quality fuels, its concentration rises[10].

### 2.1.2 Nitrogen Dioxide

In SI engines, NO<sub>2</sub> concentration is relatively small and can be neglected, but in CI, their emissions are considerably higher and must be carefully considered. The formation of NO<sub>2</sub> according to the following reactions[10]:



In diesel engines, NO<sub>2</sub> emissions become relevant when the air to fuel ratio (A/F) is high and then generally occurs at very low loads[3]. In Fig. 2.3, it is also possible to note the additional dependence on speed.

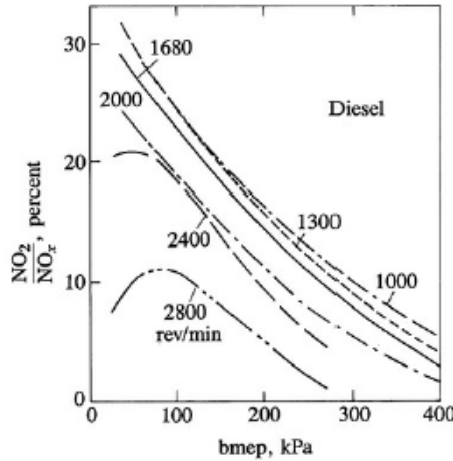


Figure 2.3: NO<sub>2</sub> concentration in different operating points[3].

### 2.1.3 NO<sub>x</sub> in Diesel Combustion

The previous section has highlighted the main requirements for NO<sub>x</sub> formation: high temperature, oxygen, and nitrogen concentration, so that chemical reactions can take place at appreciable rates according to the Zeldovich mechanism. However, as it is known, diesel combustion takes place in a heterogeneous environment since local conditions vary in space and time. Initially, it was thought that the premixed burning phase was the main responsible for NO<sub>x</sub> formation. Only in the recent past and after several laboratory investigations have been carried out, it was understood that the conditions during the premixed burning phase were unfavorable for NO<sub>x</sub> formation. It takes place under fuel-rich conditions, and the temperature in that phase typically does not exceed 1600 K. On the contrary, during the mixing controlled phase, conditions in the diffusion flame region are significantly different. Here partially burnt fuel fragments reach the flame from the inside and are eventually oxidized by the air coming from the outside[3]. The equivalence ratio  $\phi$  is near the stoichiometric value, and the energy released by the combustion raises the temperature to value required for NO<sub>x</sub> formation. However, even though the premixed combustion produces no significant amounts of NO<sub>x</sub>, the more intense is this phase, the higher will be the temperature, which activates the chemical reactions. In a diesel engine, NO<sub>x</sub> forms both in the flame front and in post flame gases, though in different amounts[3]. Since the first portions of burnt gases are further compressed, reaching higher temperatures, in post flame gases, the NO<sub>x</sub> formation is more significant[3].

## 2.2 Particulate Matter

Diesel particulate matter is made up of several chemical species aggregated in different amounts and phases. Its formation process is very complex since there is no single source, and it is further complicated by the fact that changes in composition take place along the exhaust line, from the cylinder to the atmosphere[3]. It is defined, according to EN ISO 8178, as «any material collected on a specified filter medium after diluting exhaust with clean filtered air»[11, p. 5] to a fixed temperature of  $(47 \pm 5)$  °C .

Having clarified the particulate matter definition, it is still fundamental to provide a general description of its structure. Particulate matter is the combination of a solid component (Soot) made up of carbonaceous material and a soluble part (SOF) of condensed HC and, to a minor extent, lubricant oil. It can also include low amounts of sulfate particles, depending on the sulfur content of the fuel and ash, which is mainly related to oil additives[3]. Soot forms during the premixed combustion in fuel-rich conditions when oxidation of the fuel produces fuel fragments[2]. The first step in soot formation is called nucleation and involves the arrangement in

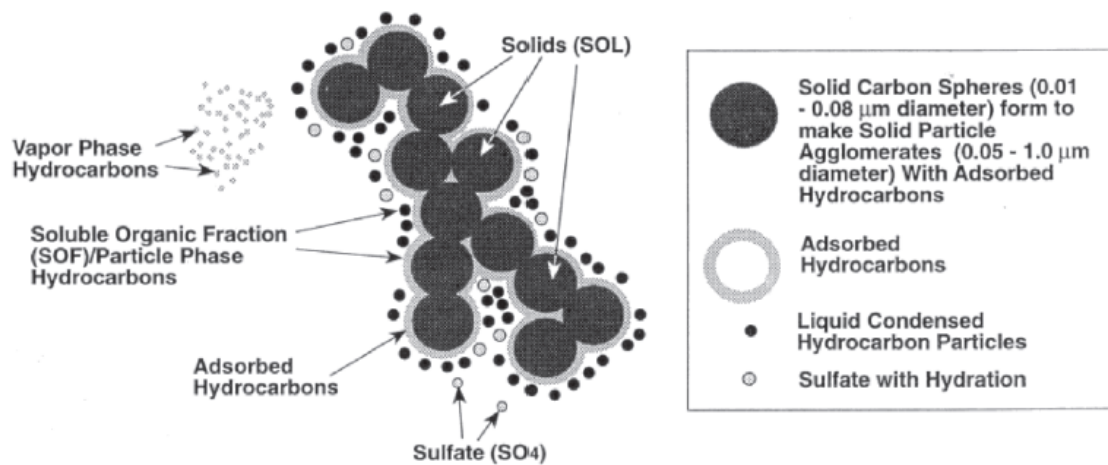


Figure 2.4: Main components of the Particulate Matter[3].

the spatial structure of the PAH[10]. They are considered as the main soot precursors since they can lead to soot formation through different mechanisms depending on the temperature at which reactions take place[3]. At temperature below 1800K, PAHs react, forming soot following a direct and fast path[3]. At higher temperatures, also aliphatic components are broken up into small fragments giving rise to soot production in an indirect way[3]. After the nucleation of the small soot particles, they may collide and forms bigger particles. This second stage is named particle growth and is further divided into coagulation and aggregation[3]. The former refers to the combination of two particles into a bigger single spherical one, while the latter describes the grouping of many small particles in a chain-like structure[3]. The last stage of particulate formation occurs in the atmosphere, once the gases have been exhausted. The absorption and condensation of material such as hydrocarbons, sulfur, and other compounds on the solid structure already formed

take place[3]. However, it should be pointed out that only a small fraction of the soot formed in the cylinder is later exhausted in the atmosphere(Fig. 2.5)[10]. This is mainly related to the oxidation of the soot particles during the whole combustion process and is also one of the reasons why the quantitative description of the soot in the exhaust is extremely complex[4].

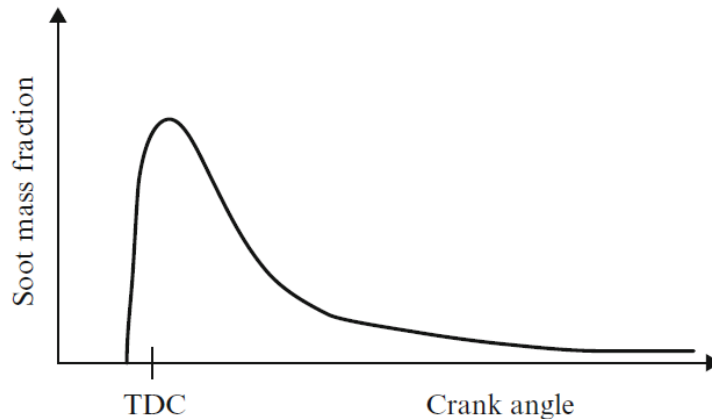


Figure 2.5: Soot mass fraction evolution in Diesel engines[10].

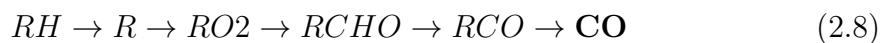
## 2.3 Unburned Hydrocarbons

Unburned hydrocarbons emissions result from all the fuel which is excluded from the primary combustion process. Apart from the emission implications, a large amount of engine-out HC impacts the overall efficiency of the combustion process. There are several mechanisms through which hydrocarbons cannot be involved in the primary oxidation process. These mechanisms are different from the ones occurring in a gasoline engine due to the different functioning of the diesel engine. In conventional diesel engines have been identified two main processes: over-mixing of the mixture resulting in too lean local mixture and under-mixing that will cause too rich zones[3]. In both cases, the local conditions are unfavourable for autoignition. Over-mixing occurs at the edge of the spray, where the equivalence ratio is very small since a large amount of hot air is available and then mix with the gaseous fuel[3]. Under-mixing depends on the fuel that enters the combustion chamber at a very low speed or on the fuel injected in an already very rich environment[3]. Since a diesel operates well lean of stoichiometric, over-mixing must be carefully

considered while under-mixing becomes an issue in transient conditions. Finally, advanced combustion strategies that require a high mixing level in order to reduce NO<sub>x</sub> or Soot have the disadvantage of enhancing HC emission.

## 2.4 Carbon Monoxide

Carbon monoxide is the result of incomplete oxidation of hydrocarbons that takes place according to the following path[3]



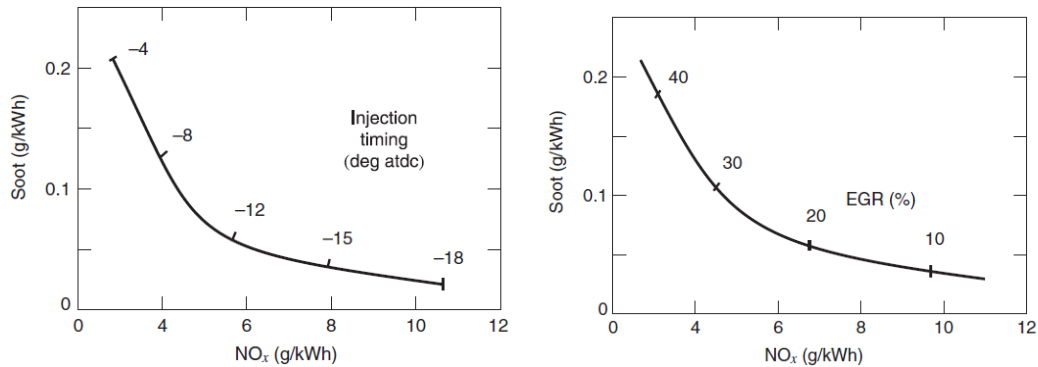
where  $R$  stands for radical. Carbon monoxide is eventually oxidized into CO<sub>2</sub>



The last equation is characterized by a lower rate constant, and then it is essentially slower than the previous ones so that when a sudden decrease of temperature freezes the chemical reaction, there is still a remaining fraction of CO not oxidized[3]. In both gasoline and diesel engines, CO emissions can be controlled mainly by A/F. Since diesel engines always operate lean, engine-out CO emissions are very low in conventional operating modes. The conditions in which they became relevant are the warm-up and the transient phases, because of fuel enrichment strategies and the conditions with high Exhaust Gas Recirculation (EGR) rates because of lack of oxygen.

## 2.5 Emissions Control

In Diesel engines, the most relevant pollutant species are NO<sub>x</sub> and PM. The common engine variables tuned in order to control and reduce their engine-out emissions are the Injection Timing and the EGR rate. It is not possible to set each of the previous parameters and achieve the simultaneous reduction of both NO<sub>x</sub> and PM, because they show opposite trends. Therefore, a trade-off strategy is required, always considering the variation of HC, CO, and other factors such as BSFC and noise[3].



(a) BSSoot vs BSNO<sub>x</sub> as a function of Injection Timing[7].

(b) BSSoot vs BSNO<sub>x</sub> as a function of EGR rate[7].

- Injection Timing

Injection timing is used to control the start of the combustion process. However, there is a certain delay between the SOI and SOC, as explained in Sec. 1.3. Advanced injection events result in longer ignition delay which in turn increases the intensity of the premixed burning phase because of better mixing between fuel and air. As a consequence, the in-cylinder temperature will be higher, enhancing NO<sub>x</sub> production. On the contrary, soot emissions will decrease because higher mixing levels reduce the local equivalence ratios. Furthermore, soot oxidation increases with higher temperatures.

- Exhaust Gas Recirculation

The EGR is an emission reduction technique developed for NO<sub>x</sub> control. A portion of the exhaust gases is drawn from the exhaust line and then recirculated inside the cylinders. The main effect of EGR is a reduction of the peak temperature achieved through the following effects: thermal, chemical and dilution[12]. The latter is the most important and consists of the oxygen replacement with inert gases, which eventually results in a broadening of the flame[12]. Nevertheless, too high EGR rate gives rise to a lack of oxygen, decreasing the oxidation of soot.

## Chapter 3

# Experimental Setup

The experimental activity has been carried out at the dynamic test bench of the Internal Combustion Engines Advanced Laboratory (ICEAL). Preliminary machining processes have been realized in order to adapt the engine systems to the laboratory's facilities and to the installation of additional measuring sensors. Then, the engine has been placed inside the test cell, connected to the dynamometer and to all the other additional systems, which will be further explained in the following sections.

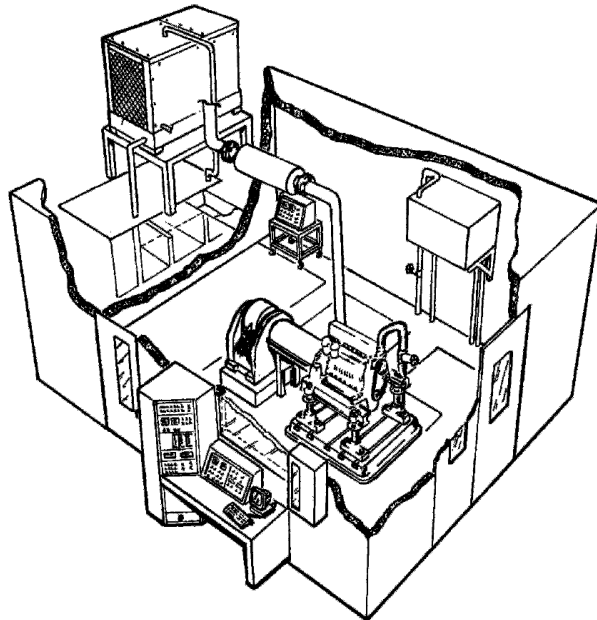


Figure 3.1: Typical experimental setup[13].

### 3.1 Test cell and Control room

The laboratory is divided into two main areas: the test cell and the control room[13]. The test cell is an open thermodynamic system whose complexity lies in the large number of subsystems that must operate simultaneously. Its fundamental elements are[13]

- Dynamometer
- Unit Under Test – UUT (Engine + Electronic control unit (ECU))
- Ventilation and air conditioning system
- Fuel supply system
- Cooling system
- Exhaust system

Furthermore, there are additional devices such as

- Measuring equipment
  - Fuel flowrate measuring system
  - Exhaust measurement system
  - Smoke meter
  - Opacity meter

- F-FEM station

It is a modular unit with all the input-output ports for data acquisition. In PUMA each port must be explicitly set with all the characteristics of the sensor, among which the most important is the calibration curve.

The control room faces the test cell and, for this reason, is acoustically isolated. It is the interface through which the operator can monitor and control the whole system. There are three main consoles equipped with

- AVL PUMA OPEN 2.0

It is the automation system for controlling and monitoring all the instrumentations and the engine under test.

- AVL INDICOM

It is used for data acquisition and management of all the information coming from the sensors.

- ETAS INCA

It is used for managing and controlling the ECU calibration parameters.

### **3.1.1 Dynamometer**

The AVL APA 100 dynamometer is installed in the test cell in order to perform the experimental tests. It is an AC asynchronous machine with a squirrel-cage rotor that can work either as a motor or generator. It has an output for each side so that two different engines can be arranged in the test cell, even if only one at a time can be directly connected to the dynamometer. The connection between engine and dynamometer is made through a removable and adjustable joint, flanged to the flywheel, and it consists of one of the most critical operations to be executed before the start of the experimental tests. The effects of an incorrect connection range from annoying noises, shaft oscillations, vibrations, and finally to failure of the test cell's equipment[13]. To avoid these kind of problems, the shaft must be properly designed in order to move its resonant frequency outside the operating range of the engine. The resonant frequency can be experimentally determined by using AVL PUMA tools that also allow continuous monitoring of the shaft state. If the difference between the dynamometer and engine speeds overcomes a limit value, PUMA switches off the engine immediately, avoiding or at least limiting possible damages. Before the dynamometer-engine coupling, the calibration of the dynamometer is needed for the measurement of the torque. The torque value is the starting point for the evaluation of all the other variables related to the engine functioning[13]. An error, although small, in this first measurement, can compromise all the subsequent activities. To perform the calibration, a weight is placed at a certain distance from the dynamometer, and the output value is measured. This operation is repeated iteratively by adding or removing the weights so that different values are investigated. Even if it seems theoretically trivial, the calibration must be carried out with the maximum carefulness. For this reason, it was commissioned to AVL's technicians.



Figure 3.2: AVL APA 100 Dynamometer[14].

### 3.1.2 Engine

The engine under test has been supplied by Fiat Powertrain Technologies (FPT). It is a four-cylinder inline 2.3 l diesel engine with common rail injection and variable geometry turbocharger (VGT) with electrical actuation. The technical characteristics are shown in Tab. 3.1. The after-treatment system consists of a DPF+DOC integrated unit. In Fig. 3.3 is also represented the SCR unit, which is used in the conventional vehicle architecture but not in the laboratory configuration. The distinctive feature of this engine is a double EGR circuit: a conventional short route circuit and a long circuit that draws the exhaust gases downstream of the ATS unit. In both circuits, there are EGR cooler units to lower down the temperature of the exhaust gases before re-entering in the cylinders.

Parameter	Unit	
Bore	<i>mm</i>	88
Stroke	<i>mm</i>	94
ConRod Length	<i>mm</i>	146
Compression ratio		16.2
TDC clearance height	<i>mm</i>	0.7
Max Power	<i>kW</i>	127
Max Torque	<i>Nm</i>	400
Eng speed at Max Torque	<i>rpm</i>	1500
Eng speed at max power	<i>rpm</i>	3600

Table 3.1: Engine parameters.

### 3.1.3 Cooling System

The engine installed on the test bench is not coupled with a radiator. Then, the test cell must provide an external cooling system capable of performing all the tasks of a conventional one without affecting the meaningfulness of the tests[15]. In the ideal case, it would be able to replicate the effect of the radiator in all the working conditions[15]. Since this is not possible, then the goal is to maintain the coolant at a constant  $\Delta T$  between engine inlet and outlet. The cooling system components are[15]

- Air-Liquid Heater  
It is used during warm-up to increase coolant temperature.
- Liquid-Liquid Heat exchanger  
It performs the functions of a conventional radiator.
- Recirculation Pump  
The pump is placed downstream of the radiator in order to offset the losses inside the circuit.

## 3.2 Sensors for data acquisition

In this section, all the different types of sensors that were installed on the engine will be explained both from a theoretical and technical point of view. One critical point of each sensor's installation phase was the evaluation of the calibration curve and, eventually, its upload on PUMA system for a reliable and precise measurement.

### 3.2.1 Pressure sensors

Differential pressure sensors are made up of a diaphragm on which several piezo resistors are connected in a proper electrical circuit[16]. The pressure difference between the two faces of the diaphragm gives rise to the deformation of the resistors causing changes in their resistance. Then the voltage signal measured at the terminals of the circuit is a function of the pressure. The pressure sensors installed on the engine have different characteristics that are listed in Tab. 3.2.

Table 3.2: Kistler pressure sensors characteristics[17].

Sensor Model	Measuring Range	Temperature Range	Natural Frequency	Cooling Fluid Flow
	bar	°C	kHz	l/min
4007C	0 to 250	-40 to 200	>100	-
6058A	0 to 250	-20 to 350 -50 to 400	160	-
4049B	0 to 5/10	0 to 120	> 60	0.3-0.5

### 3.2.2 Temperature sensors

Thermocouples exploit the Seebeck effect on the conversion of heat into electricity[16]. The thermal gradient across an electrical conductor results in a potential difference because of the electrical current generated in the conductor itself[16]. In practical applications, such as automotive sensors, two different conductors in contact are used, and the voltage between them is measured. Typically, this voltage is very small, and then an amplifier is needed. From a technical point of view, there are different types of thermocouples, mainly depending on their construction material and the temperature range. On the F1A engine have been installed thermocouples of types T and K("see Appendix A"), whose standard characteristics are listed in Tab. 3.3.

Table 3.3: Thermocouples characteristics[18, p. 4].

Type	Lead Metal A (+)	Lead Metal B(-)	Range [°C]	EMF over range [mV]	Seebeck coefficient [ $\mu V/^\circ C$ at 0 °C]
K	Chromel	Alumel	-270 to 1370	-6.458 to 54.886	39.48
T	Copper	Constantan	-200 to 400	-6.258 to 20.872	38.74

### 3.2.3 Mass Air Flow Sensor

Mass airflow meter is also known in the automotive field as a hot wire sensor. It is based on heat exchange between the hot wire and the airflow under the assumption that heat transfer occurs only by convection[16]. Arranging the resistor in a proper circuit, it is possible to keep its temperature almost constant so that the current flowing in the circuit is proportional to the mass flow.

### **3.2.4 Exhaust Gas Analyzers**

An Exhaust Gas Oxygen sensor is installed downstream of the turbine just before the ATS unit. Its measurements provide a reliable index of the  $\lambda$  value inside the combustion chamber, typically in the range of  $0.7 < \lambda < \infty$ [9]. It is made up of a Zirconium Dioxide plate with two electrically insulated platinum electrodes at its opposite ends. One electrode faces the exhaust gas stream while the other the atmospheric air[16]. According to the Nernst principle, Zirconium Dioxide has the property of attracting oxygen ions. Since the air oxygen concentration is much higher than in the exhaust, more ions accumulate on the air electrode giving rise to the potential difference that is measured as an index of oxygen concentration.

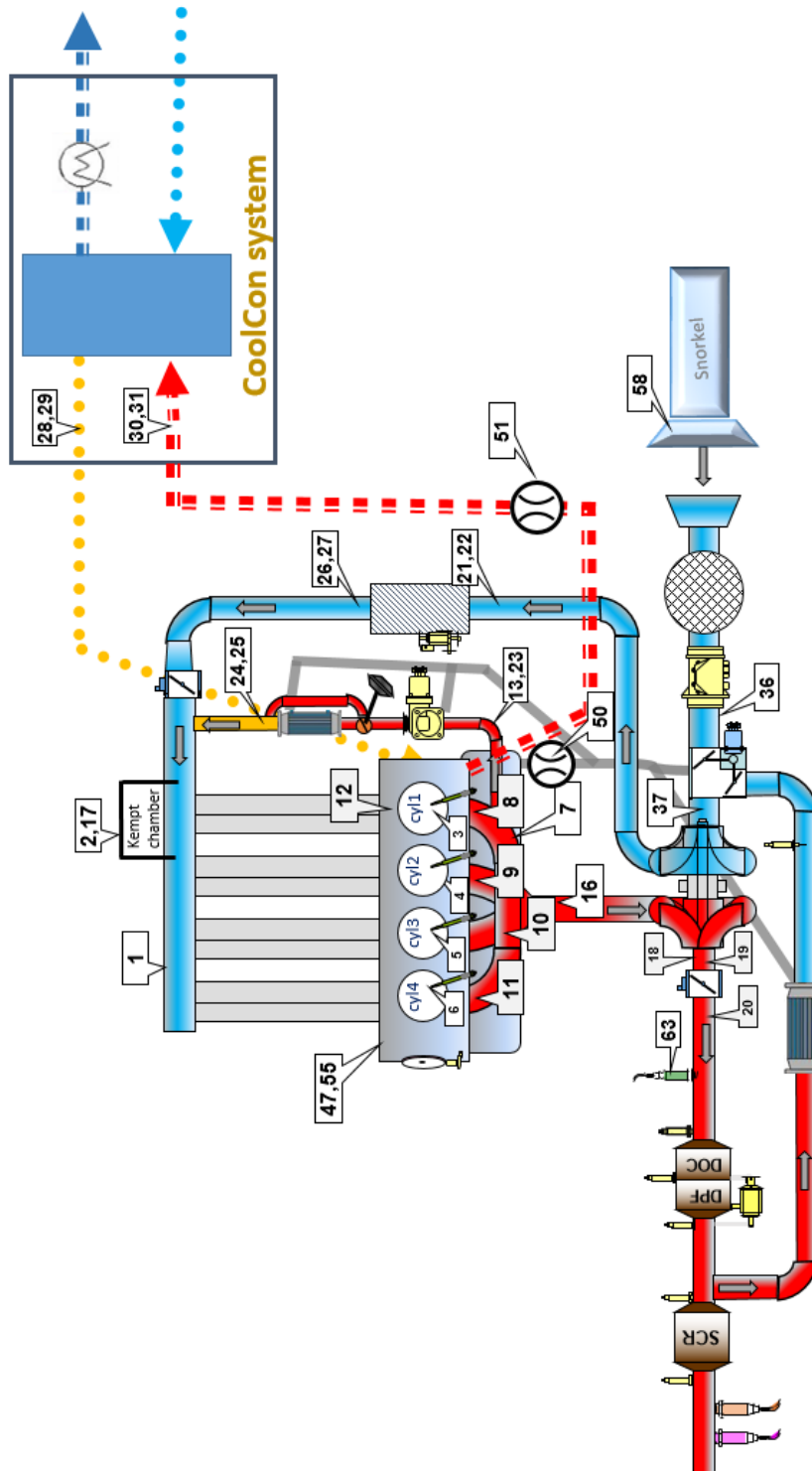


Figure 3.3: F1A architecture and sensors positioning.

### 3.3 Fuel Metering System

The AVL KMA 4000 is used for fuel consumption measurement given its high reliability, flexibility, and precision that are a direct consequence of the PLU measuring principle[14]. The PLU positive displacement meter assures a zero pressure drop between the inlet and outlet of the gear meter thanks to a bypass line in which the position of a piston is used as an input signal for the servo-controlled motor that drives the gear meter whose speed is continuously adjusted[14]. In this way, there is zero difference between the inlet and outlet flow, which is zero leakage losses, and the measurement is independent of density, viscosity, and temperature of the fuel.



Figure 3.4: AVL KMA 4000[14].

### 3.4 Emissions measurement equipment

The AVL AMAi60 is a compact unit that includes the technical instruments for the measurement of the pollutant emissions. It performs a raw analysis of the exhaust gases by using the following devices:

- Non-Dispersive Infrared Analyzer
- Chemiluminescence Detector
- Flame Ionization Detector

- Paramagnetic Detector

Particulate matter is measured by using

- AVL 415S - Opacimeter
- AVL 439 - Smokemeter

The AVL AMAi60 is connected to three independent measurement heated lines, each with a different sampling point on the circuit. The first line extracts the gas before the ATS providing the engine out concentrations, the second line after the ATS returning the tailpipe emissions, and finally, the third one allows the measurement of the CO<sub>2</sub> concentration at the intake for the calculation of the EGR rate. All the instruments must be cleaned and calibrated before starting the experimental tests. Furthermore, once the tests have already started and after a certain number of consecutive measurements, gas is pushed into the sampling lines in order to remove the residual gases from the analyzers[19].

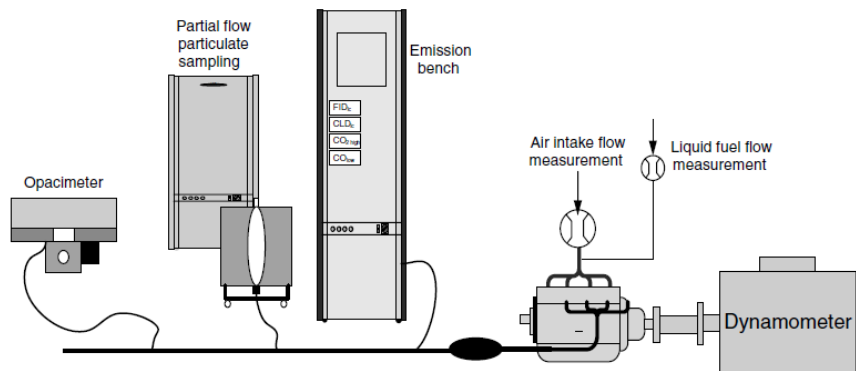


Figure 3.5: Typical measuring line[19].

### 3.4.1 Non-Dispersive Infrared Analyzer

Non-Dispersive Infrared Analyzer is used in automotive applications for measuring mainly CO and CO<sub>2</sub> concentrations in the exhaust gases. Its operating principle is based on the absorption of infrared radiation within a specific wavelength by multi atom gases[20]. To identify precisely the gas and to measure its concentration, the gas must have a distinctive spectrum in which there is no overlap with other gases. The main issue related to such an analyzer is the impact on measurements

of the water content in the gas since  $H_2O$  has a vast spectrum, and they can alter the concentration of the investigating gas[20]. For this reason, NDIR typically performs dry analysis or use particular countermeasures to determine the water content[20]. In the figure, an infrared light source faces two independent cells[20]. The so-called reference cell contains nitrogen, an inert gas that does not absorb a significant amount of radiation, while the absorption one is fed with the sample of gas. The infrared radiation emitted by the source goes through both the cells and eventually arrives at a detector device, filled with the gas to be analyzed. A diaphragm splits the detector into two chambers, one facing the reference cell and the other one the absorption cell. The gas inside the absorpction subtracts energy from the light beam resulting in different heating of the detector's chambers. A pressure difference arises between them, and the diaphragm deformation is eventually converted into an electrical signal proportional to the gas concentration. The modulation of the signal is obtained by using a rotating chopper, which makes the light beam intermittent[19].

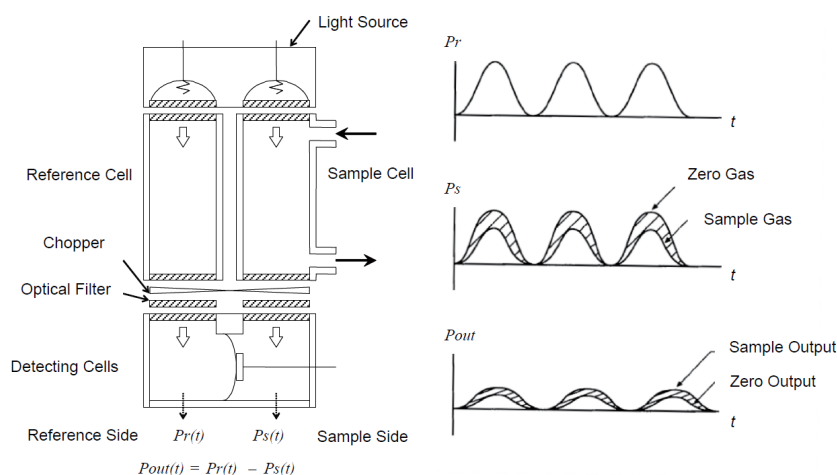


Figure 3.6: Non-Dispersive Infrared Analyzer[20].

### 3.4.2 Chemiluminescence Analyzer

CLD instruments are designed to measure  $NO$  concentration in a sample gas. The core of the CLD is the reaction chamber, where the chemical reactions between  $NO$  and the ozone take place giving as a product  $NO_2$  particles electrically energized. Eventually, these particles will return to a basic state throughout the emission of

light (chemiluminescence) which is then captured by a photomultiplier positioned inside the device. The reactions between NO and O<sub>3</sub> are[7]



The overall nitrogen oxides concentration is moderately affected by NO<sub>2</sub> content in the sample. For this reason, a NOx converter unit reduces NO<sub>2</sub> into NO before the CLD's reaction chamber so that it is possible to measure the overall NOx emissions[20]. It is also possible to obtain the emissions of NO and NO<sub>2</sub> individually. In this case, the complexity of the CLD increases because it requires two separate lines: on the first one, a conventional device measures nitric oxides concentration while on the second line, a converter unit allows measuring the total nitrogen oxides content[20]. Finally, NO<sub>2</sub> are the difference between NOx and NO.

The main issue related to CLD is the quenching effect as a result of the CO and H<sub>2</sub>O concentrations in the sample gas[20]. They react with NO<sub>2</sub> inhibiting the light emission. One of the practical solutions for the quenching effect is a vacuum reaction chamber so that the gas density decreases as does the unwanted reactions[20].

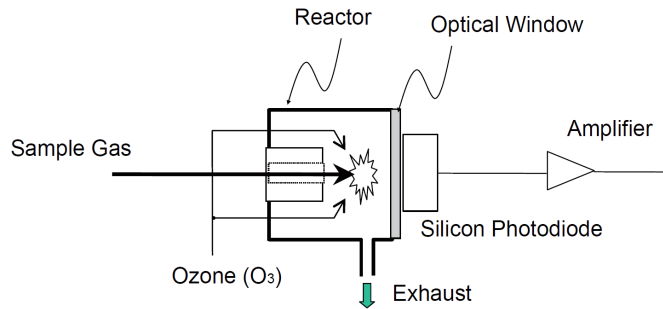
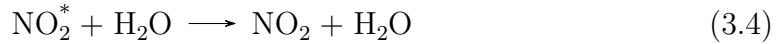


Figure 3.7: ChemiLuminescence Detector[20].

### 3.4.3 Flame Ionization Detector

FID is used for measuring the total hydrocarbon content emitted by the engine. Its working principle is based on the awareness the combustion of hydrocarbons yields a considerable amount of ions proportional to the carbon atoms. The simplest version of FID consists of a collector cell in which a hydrogen/helium flame burns between two electrodes at a constant electrical potential[20]. The hydrogen/helium mix is chosen because it does not produce any considerable amount of ions so that when the sample gas is injected in the burning flame, the ions production generates a current flow between the two electrodes that is only ascribed to the carbon content in the sample gas. The relation between total hydrocarbon concentration and the output current is almost linear, but it must be properly calibrated before the measurements with a gas of known carbon content that is taken as a reference. Then, the instrument returns a value expressed in units of reference gas or ‘ppmC’, obtained by multiplying the volume concentration and the average number of carbon atoms in the HC[20].

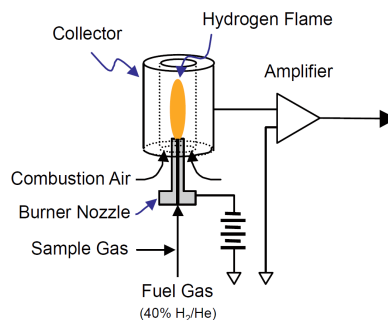


Figure 3.8: Flame Ionization Detector[20].

### 3.4.4 Paramagnetic Detector

These kinds of devices exploit the paramagnetic property of oxygen. O<sub>2</sub> particles in a magnetic field align according to the direction of the field and enhance its strength. Paramagnetic detectors are today available in different configurations. The device in Fig. 3.9 is built up using an electromagnet and a chamber provided with a specific detector[20]. The oxygen in the sample gas produces a pressure increase near the magnetic pole, depending on its concentration. Then, the pressure is converted by the detector in an electrical signal that is related to the oxygen content.

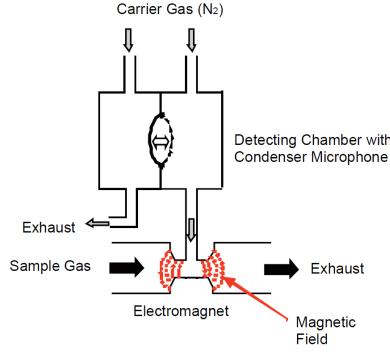


Figure 3.9: Paramagnetic Detector[20].

### 3.4.5 Particulate Analyzers

As explained in Chapter 2, particulate has a complex chemical composition, and therefore it can be classified considering several properties. The main ones are particle mass, particle number, and the smoke intensity. Each of them must be investigated using a particular measuring technique and the relative instrument. The testing equipment in the laboratory includes a smoke meter and an opacity meter for measuring the engine out smoke emissions. Both instruments use optical techniques, but they are significantly different. In a smoke-meter a portion of the exhaust gas passes through a removable white paper filter. At the end of the test, the filter is extracted and positioned between a light source and a receiver. The latter captures the amount of reflected light so that the blackening degree due to the smoke concentration is linked to a reduction of the light intensity[20]. Typically, the result of these measurements is expressed in a Bosch scale that ranges between 0 and 10 Filter Smoke Number(FSN) , according to the standard ISO 8178[11]

$$FSN = \left( \frac{1 - R'_b}{R'_c} \right) \quad (3.5)$$

where  $R$  is the reflectometer value and the subscripts  $b, c$  refer to the blackened and clean filter respectively.

As it is clear, the smoke meter cannot be used for continuous exhaust analysis since each measurement requires filter removal. The opacity meter is characterized by a sampling channel through which a portion of exhaust gas flows. The presence of soot in the exhaust stream results in a difference between the light emitted by

a source and that measured by a receiver[20]. The standard ISO 11614 defines the opacity as «the fraction of light transmitted from a source through a smoke obscured path, which is prevented from reaching the observer or the instrument receiver»[21, p. 2] and is computed as

$$N = 100 - \tau = 100 - \frac{I}{I_0} 100 \quad (3.6)$$

This kind of measure is affected by the length of the light path, the temperature, and pressure of the gas[21].

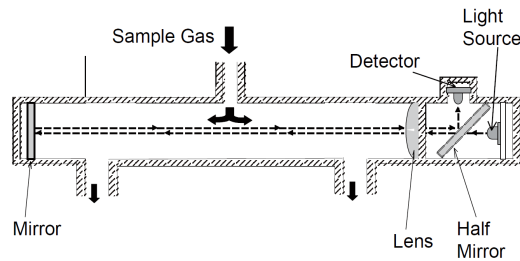


Figure 3.10: Opacity meter[20].

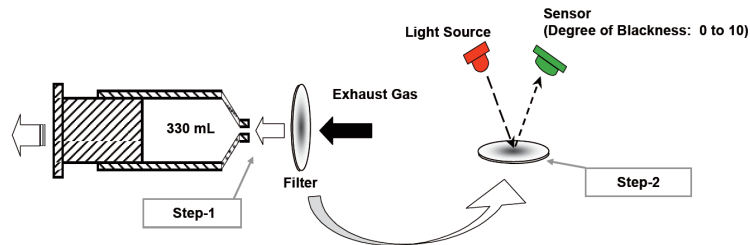


Figure 3.11: Smoke meter[20].

# Chapter 4

## Results

The final part of the experimental activity focused on the investigation of the Dual Loop EGR system. As described in Fig. 3.3, the engine is equipped with a conventional High-Pressure circuit that draws the exhaust gases upstream of the turbine inlet and then brings them to the intake manifold. Furthermore, there is an additional Low-Pressure EGR circuit based on the extraction of the exhaust gases downstream of the ATS unit.

Table 4.1: Values of the main test variables. O=Open and C=Closed.

Description	Unit	PUMA name	Value
SOI	°	#phi SOI P1	-2.9
Rail pressure	bar	#p rail	610
Exhaust Flap	-		0 [O]
Throttle Valve Actuator	-	ThrVlv_rDesVal	0 [O]
VGT Actuator	-	TrbCh_rDesVal	88 [O=0; C=100]
Pilot injection 1 mass quantity	mg/c	InjCrv_qPiI1Des_mp	1.95
Pilot injection 2 mass quantity	mg/c	InjCrv_qPiI2Des_[0]	0.7
Desired time component for Pilot 1 start of energizing	$\mu s$	InjCrv_tiPiI1Des	1090
Desired time component for Pilot 2 start of energizing	$\mu s$	InjCrv_tiPiI2Des	2240
Main injection 1 mass quantity	mg/c	InjCrv_qMI1Des	3.6

The experimental tests were executed considering one engine operating point of 2 bar bmep(1250 rpm x 34 Nm). The variables in Tab.4.1 were fixed, and two different sets of tests were performed in the following manner: the first test of each

set was run by using only one EGR circuit, and in the following test this circuit was partially closed while the other one was being opened increasingly. The first value of the air to fuel ratio in each set was recorded, and it varied in a limited range in the following tests. The opening of the HP and LP valves was regulated so that the two circuits were operated simultaneously or individually (Tab.4.2).

Table 4.2: Test plan.

Test number	Relative Air/Fuel ratio	HP EGR	LP EGR
16		100	0
17		50	80
18	$\lambda = 2.67 \pm 0.015$	30	82
19		15	84.5
20		0	91.5
21		0	98
22	$\lambda = 2.10 \pm 0.015$	15	90.5
23		30	88
24		50	86

In Fig.4.1, the temperature in the intake manifold is a function of the HP-LP EGR valves combinations. The temperature of the exhaust gases drawn before the turbine is very high so that by increasing the opening of the HP EGR valve, a large amount of hot gases is routed to the intake manifold, causing the temperature to rise. On the contrary, LP EGR has a cooling effect on the HP EGR portion that is beneficial in terms of intake manifold temperature.

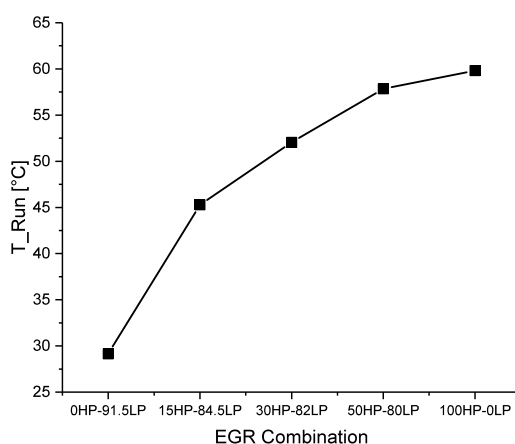


Figure 4.1: Temperature inside the intake manifold for different HP-LP combinations.  $\lambda = 2.67 \pm 0.015$

The NO<sub>x</sub> trend in Fig.4.2 is similar to previous one. The HP EGR rate increase leads to more substantial NO<sub>x</sub> emissions because of the higher temperature of the intake charge. As a consequence, the LP EGR circuit results in the opposite trend.

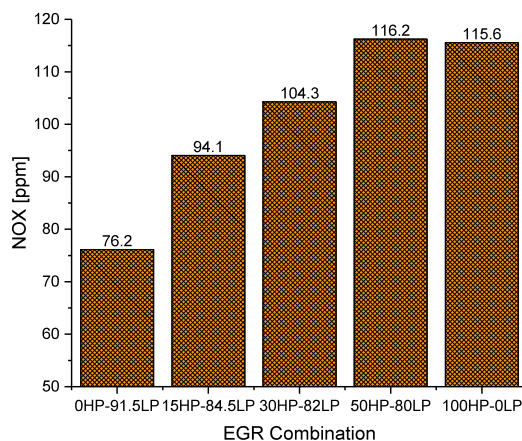


Figure 4.2: Nitrogen Oxides emissions for different HP-LP combinations.  $\lambda = 2.67 \pm 0.015$

The analysis of the pumping work(Fig.4.3) is strictly related to the pressure difference between the exhaust and intake manifolds that, in turn, is significantly affected by the positions of the throttle valve, the exhaust flap, and the VGT. In the test carried out during this activity, these variables were fixed. For this reason, the variations in the pmep, although small, might be ascribed mainly to changes in the gas flow inside the circuit, depending on the relative opening of HP and LP valves.

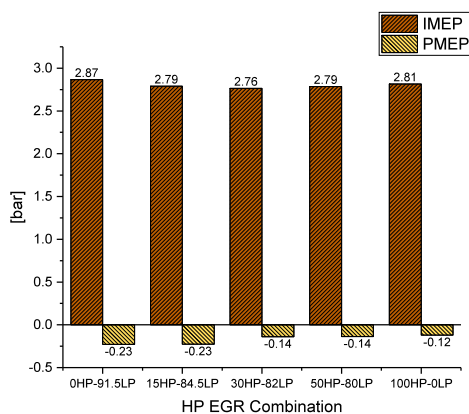


Figure 4.3: Cylinder # 1 IMEP and PMEP for different HP-LP combinations.  $\lambda = 2.67 \pm 0.015$

The BSFC in Fig.4.4 is almost constant over the different tests. However, when the two systems operate individually, the BSFC increases probably because of the combustion process worsening.

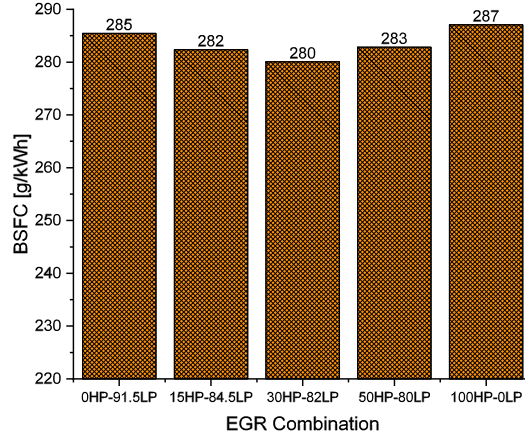


Figure 4.4: Brake specific fuel consumption for different HP-LP combinations.  $\lambda = 2.67 \pm 0.015$

The LP EGR impacts on the net heat release rate because of its effect on the intake charge temperature. Therefore, the combustion process is characterized by a longer ignition delay. This effect can be easily detected when the two circuits are operated individually, as it is shown in Fig.4.5, while it is less evident for DL EGR operations.

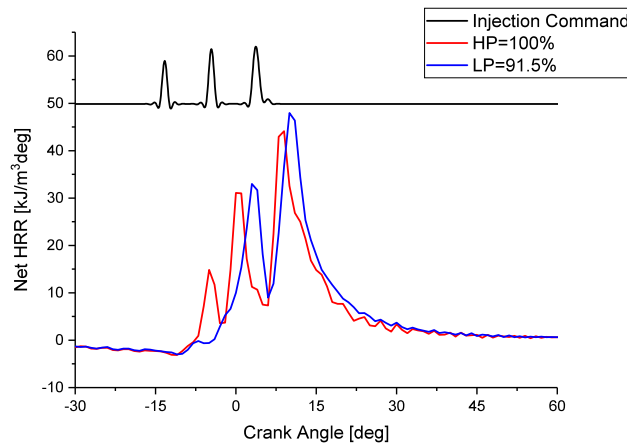


Figure 4.5: Net Heat-Release Rate of cylinder #1 for different HP-LP combinations.  $\lambda = 2.67 \pm 0.015$

In cases of longer ignition delay, the center of combustion MBF50 is reached further away from the TDC (Fig.4.6). In future experimental tests, it will be necessary to advance the start of injection properly when using the LP system to reach also a stable combustion process.

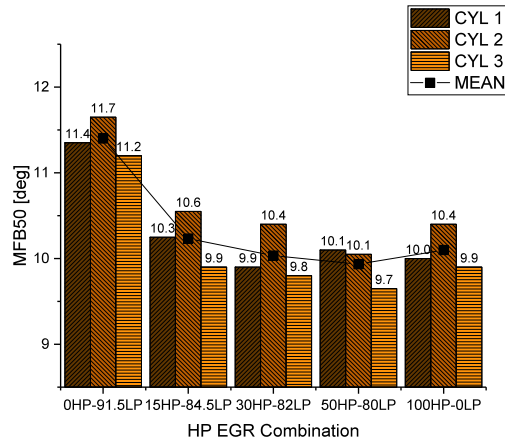


Figure 4.6: Center of combustion MFB50 for different HP-LP combinations.  $\lambda = 2.67 \pm 0.015$

## 4.1 Combustion process

### 4.1.1 In-cylinder pressure

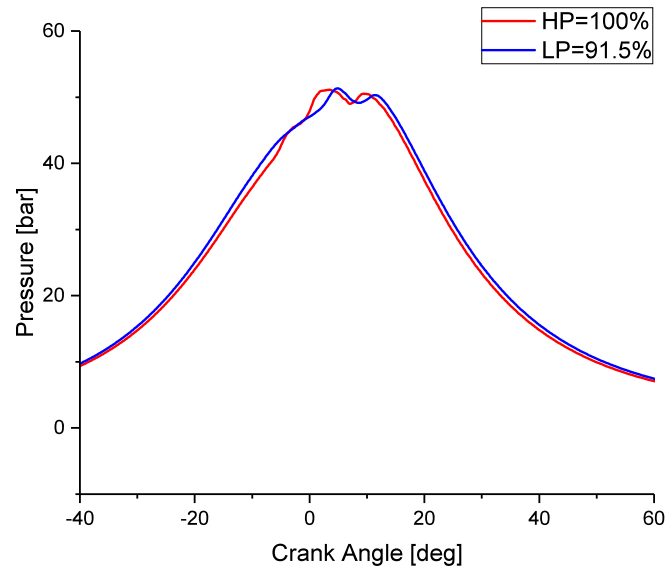


Figure 4.7: In-cylinder #1 pressure for different HP-LP combinations.  $\lambda = 2.67 \pm 0.015$

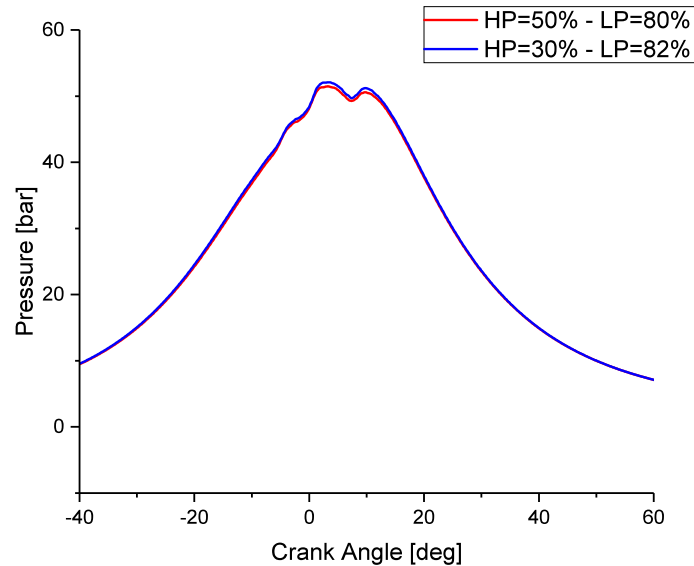


Figure 4.8: In-cylinder #1 pressure for different HP-LP combinations.  $\lambda = 2.67 \pm 0.015$

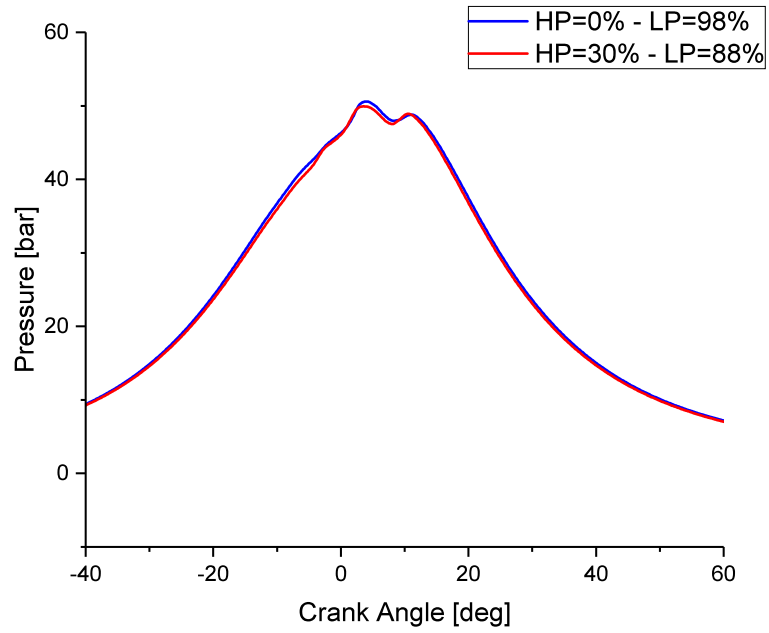


Figure 4.9: In-cylinder #1 pressure for different HP-LP combinations.  $\lambda = 2.10 \pm 0.015$

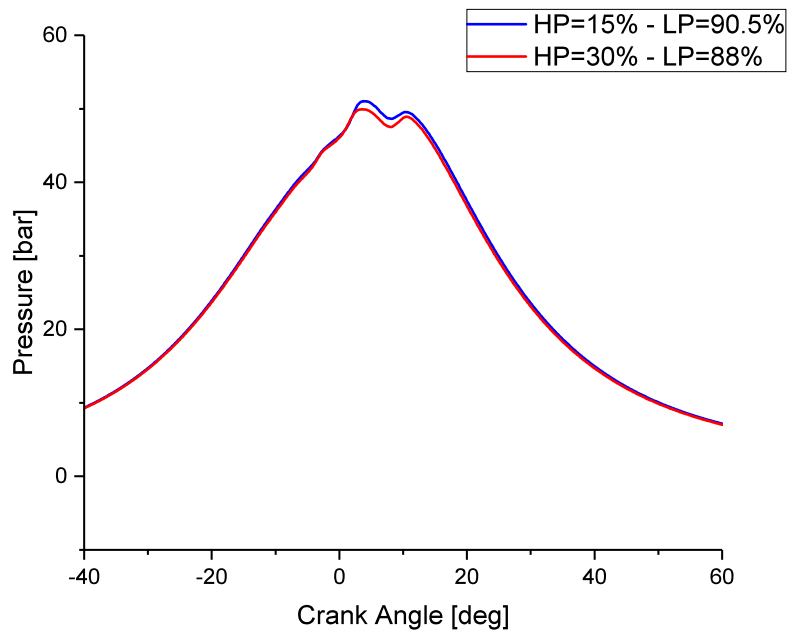


Figure 4.10: In-cylinder #1 pressure for different HP-LP combinations.  $\lambda = 2.10 \pm 0.015$

### 4.1.2 Net Heat-Release Rate

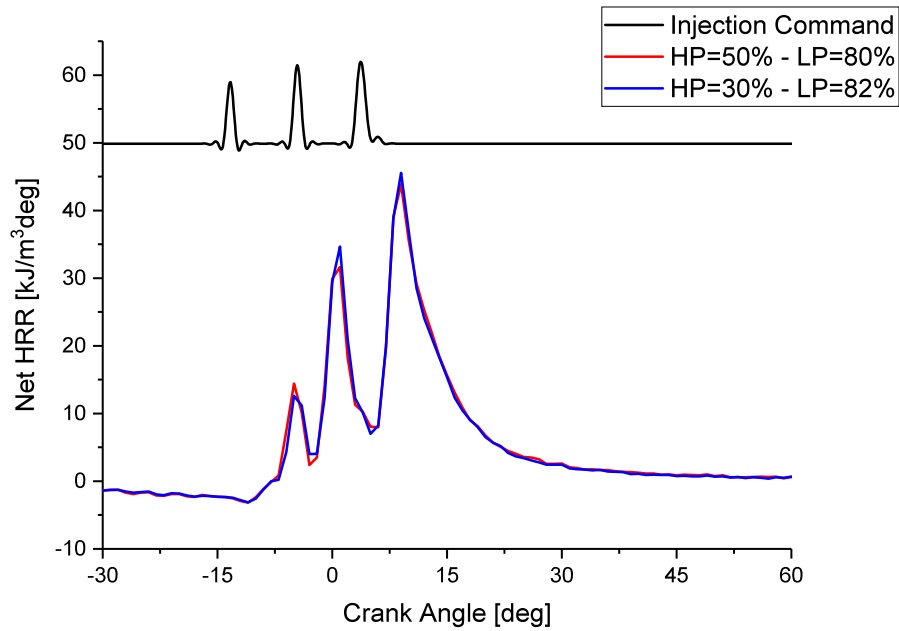


Figure 4.11: Net Heat-Release Rate of cylinder #1 for different HP-LP combinations.  $\lambda = 2.67 \pm 0.015$

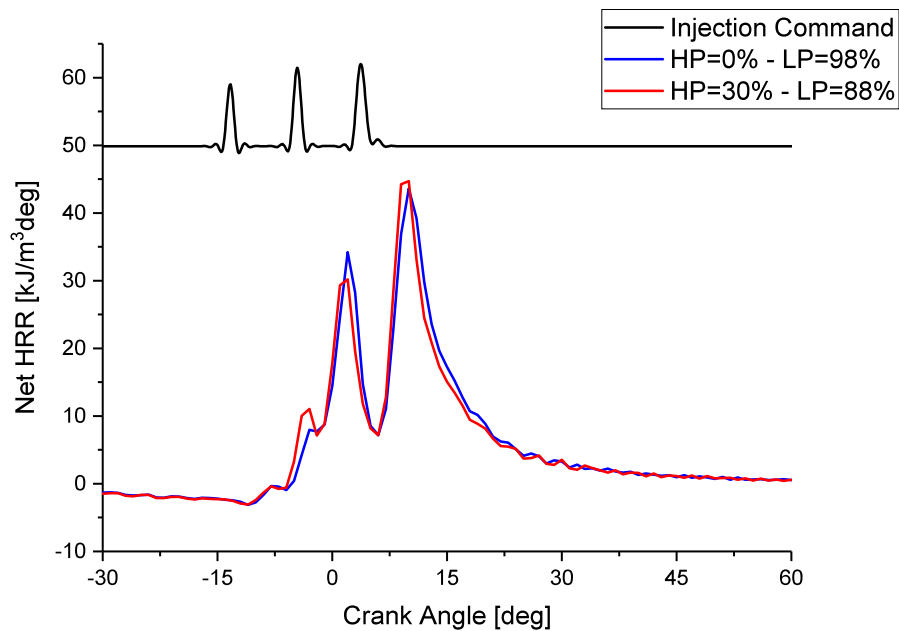


Figure 4.12: Net Heat-Release Rate of cylinder #1 for different HP-LP combinations.  $\lambda = 2.10 \pm 0.015$

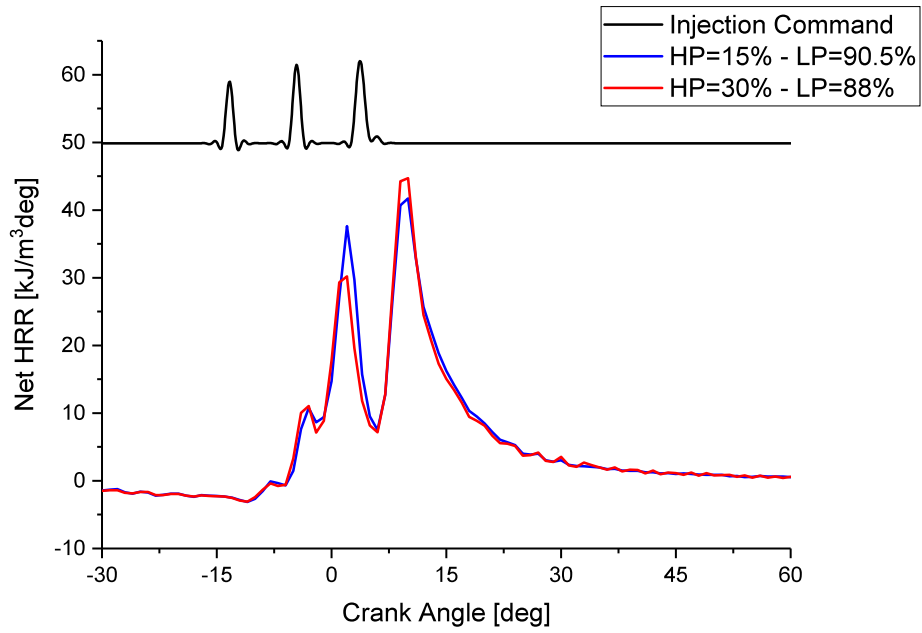


Figure 4.13: Net Heat-Release Rate of cylinder #1 for different HP-LP combinations.  $\lambda = 2.10 \pm 0.015$

### 4.1.3 Cumulative Heat-Release Rate

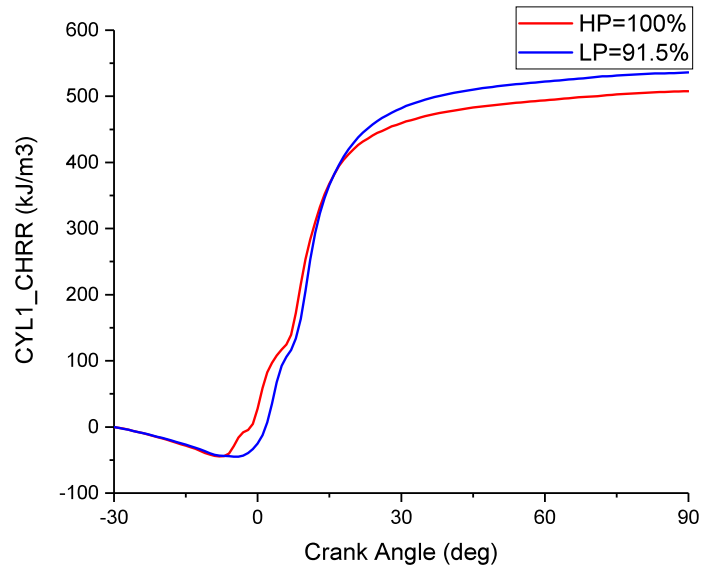


Figure 4.14: Cumulative Heat-Release Rate of cylinder #1 for different HP-LP combinations.  $\lambda = 2.67 \pm 0.015$

#### 4.1.4 Brake specific fuel consumption, Coefficient of variation and MFB50

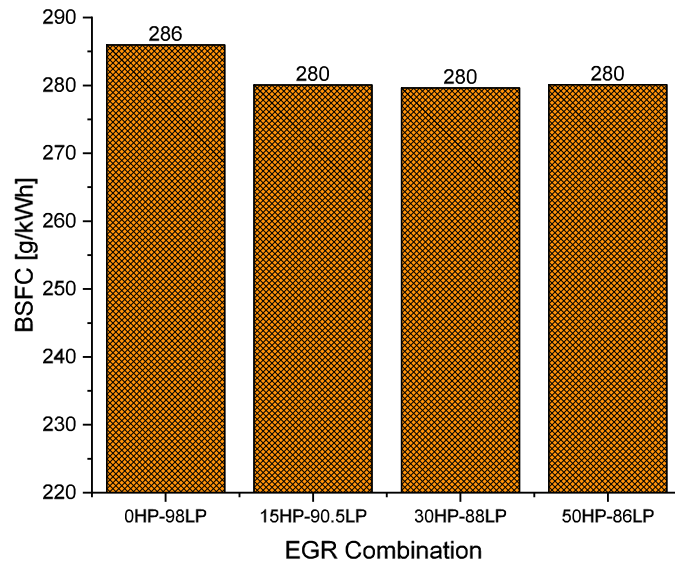


Figure 4.15: Brake specific fuel consumption for different HP-LP combinations.  $\lambda = 2.10 \pm 0.015$

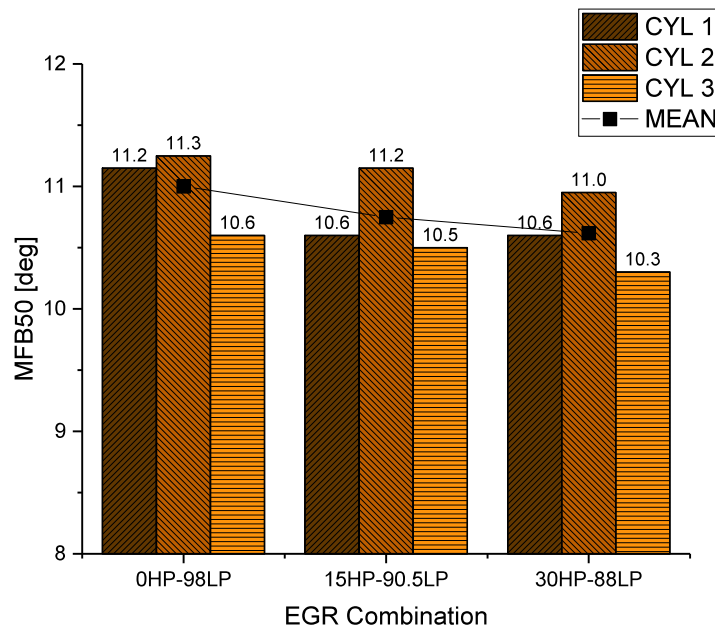


Figure 4.16: Center of combustion MFB50 for different HP-LP combinations.  $\lambda = 2.10 \pm 0.015$

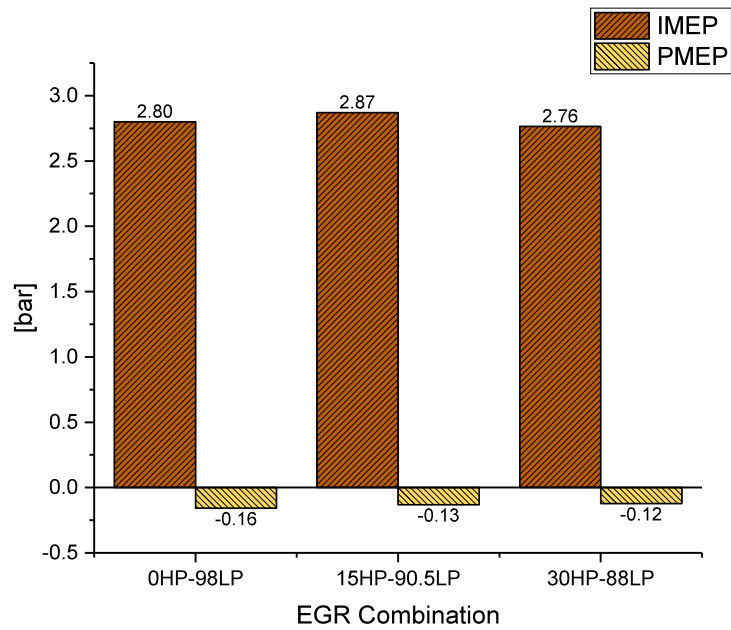


Figure 4.17: Cylinder # 1 IMEP and PMEP for different HP-LP combinations.  $\lambda = 2.10 \pm 0.015$

## 4.2 Pollutant Emissions

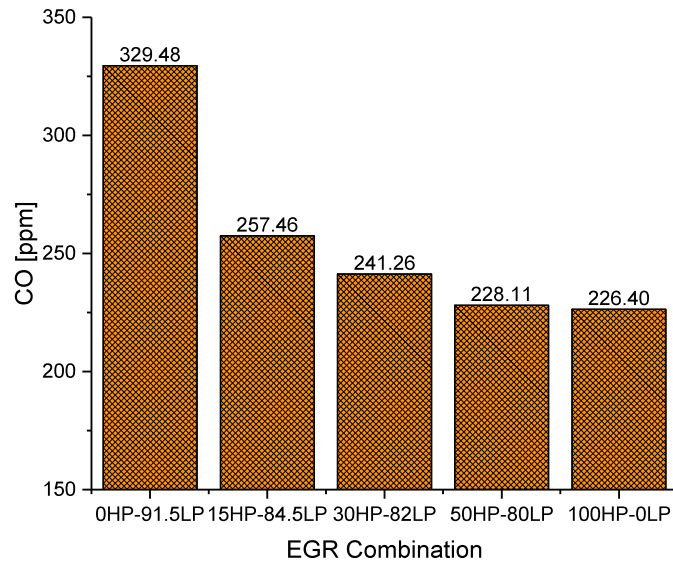


Figure 4.18: Carbon Monoxide emissions for different HP-LP combinations.  $\lambda = 2.67 \pm 0.015$

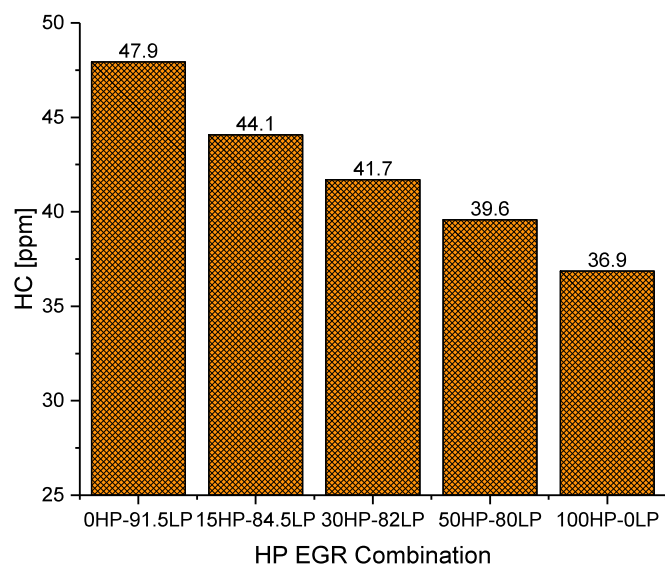


Figure 4.19: Unburned Hydrocarbons emissions for different HP-LP combinations.  $\lambda = 2.67 \pm 0.015$

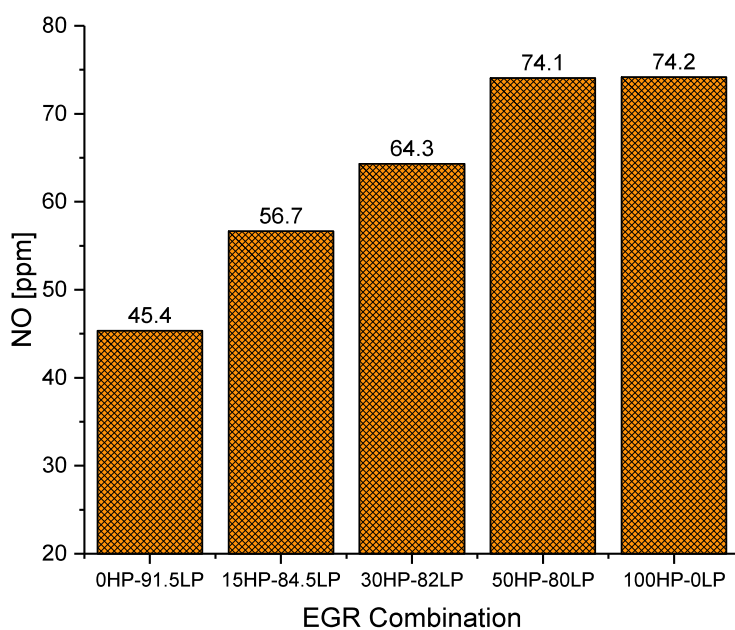


Figure 4.20: Nitric Oxide emissions for different HP-LP combinations.  $\lambda = 2.67 \pm 0.015$

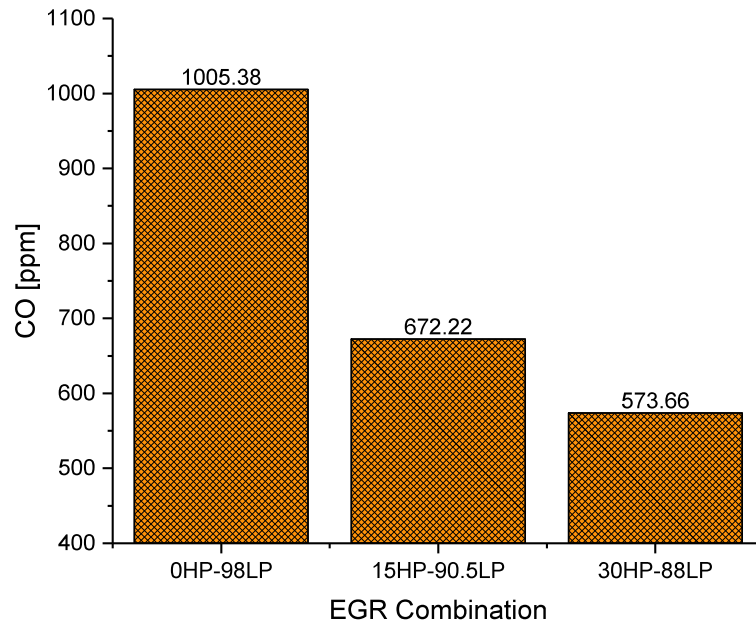


Figure 4.21: Carbon Monoxide emissions for different HP-LP combinations.  $\lambda = 2.10 \pm 0.015$

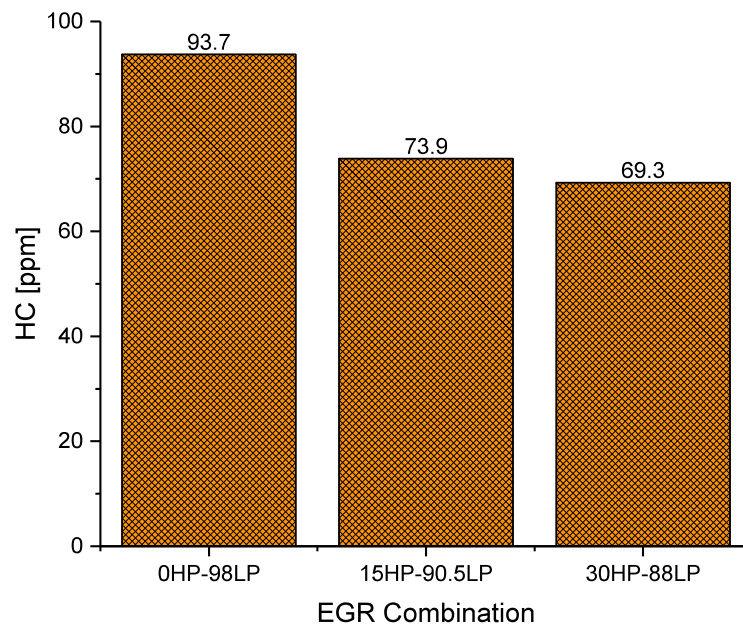


Figure 4.22: Unburned Hydrocarbons emissions for different HP-LP combinations.  $\lambda = 2.10 \pm 0.015$

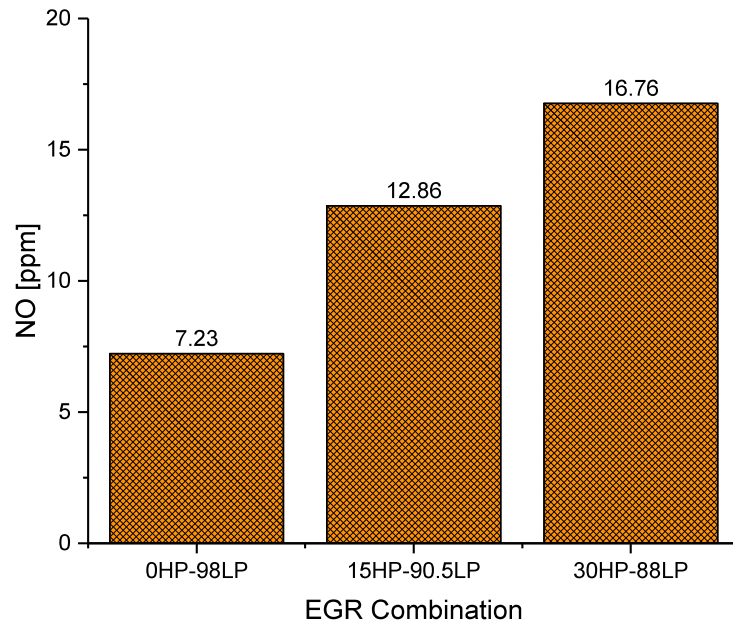


Figure 4.23: Nitric Oxide emissions for different HP-LP combinations.  $\lambda = 2.10 \pm 0.015$

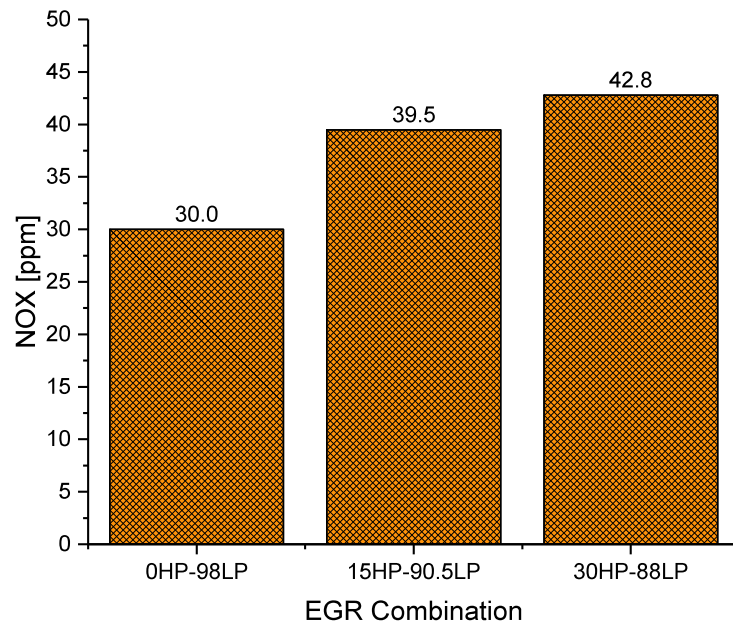


Figure 4.24: Nitrogen Oxides emissions for different HP-LP combinations.  $\lambda = 2.10 \pm 0.015$

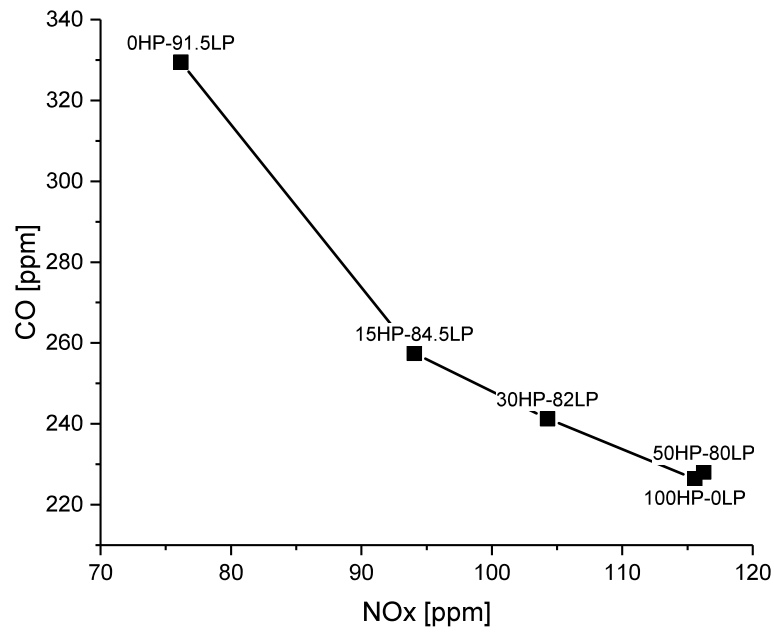


Figure 4.25: NOx vs HC trade-off for different HP-LP combinations.  $\lambda = 2.67 \pm 0.015$

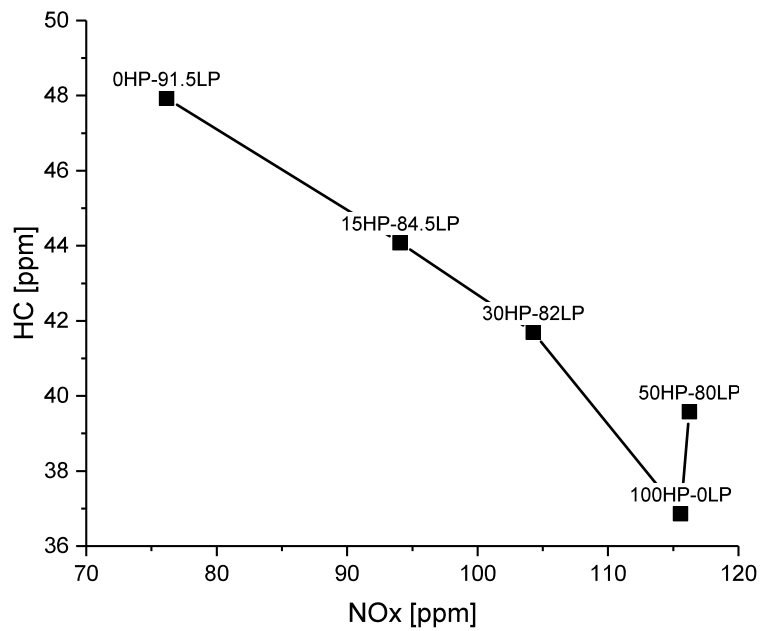


Figure 4.26: NOx vs HC trade-off for different HP-LP combinations.  $\lambda = 2.67 \pm 0.015$

### 4.3 System parameters

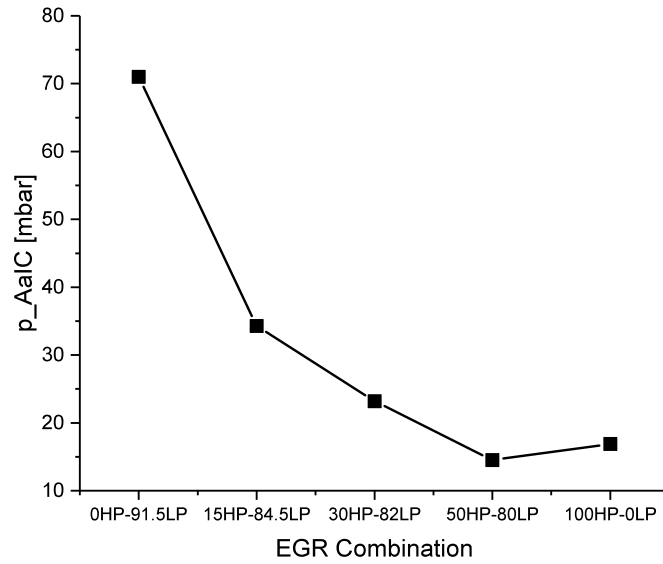


Figure 4.27: Air pressure after Inter-cooler for different HP-LP combinations.  $\lambda = 2.67 \pm 0.015$

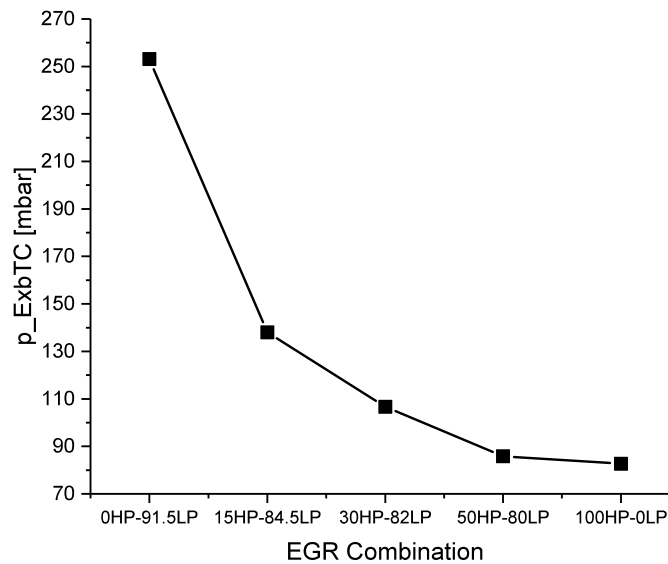


Figure 4.28: Exhaust pressure before turbocompressor for different HP-LP combinations.  $\lambda = 2.67 \pm 0.015$

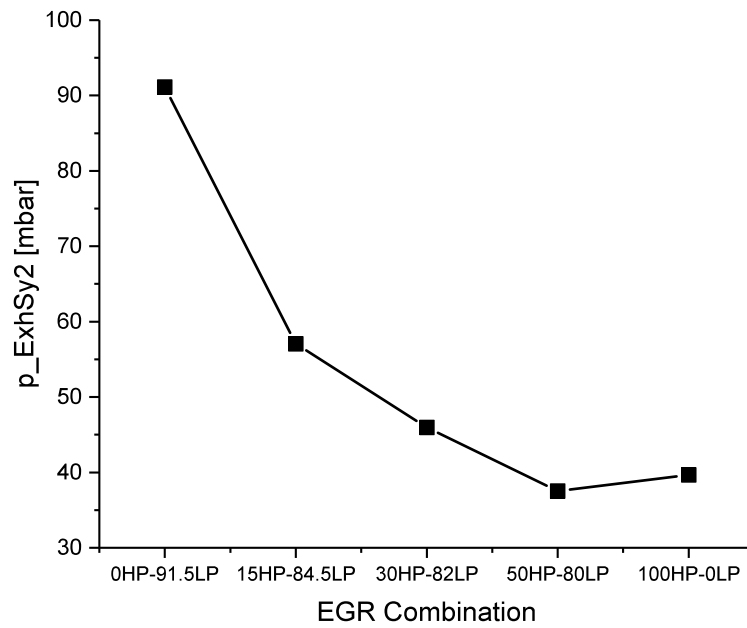


Figure 4.29: Pressure after HP EGR cooler for different HP-LP combinations.  
 $\lambda = 2.67 \pm 0.015$

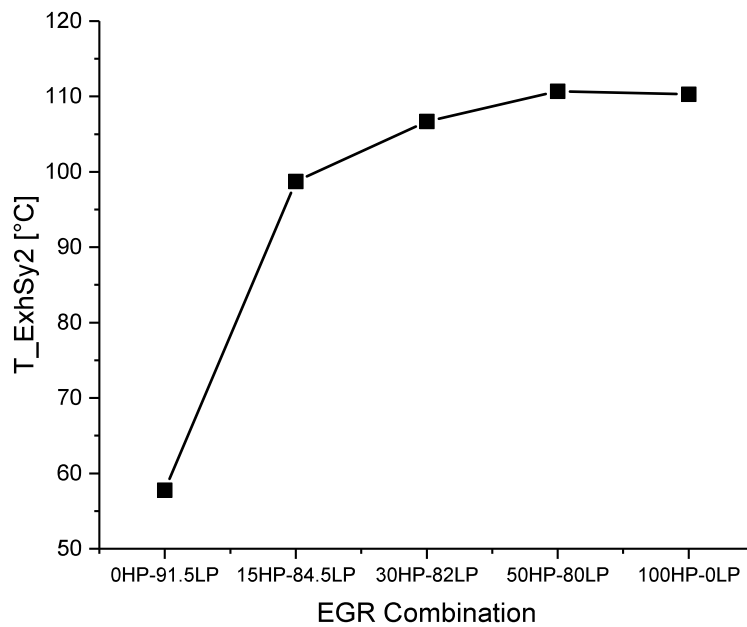


Figure 4.30: Temperature after HP EGR cooler for different HP-LP combinations.  
 $\lambda = 2.67 \pm 0.015$

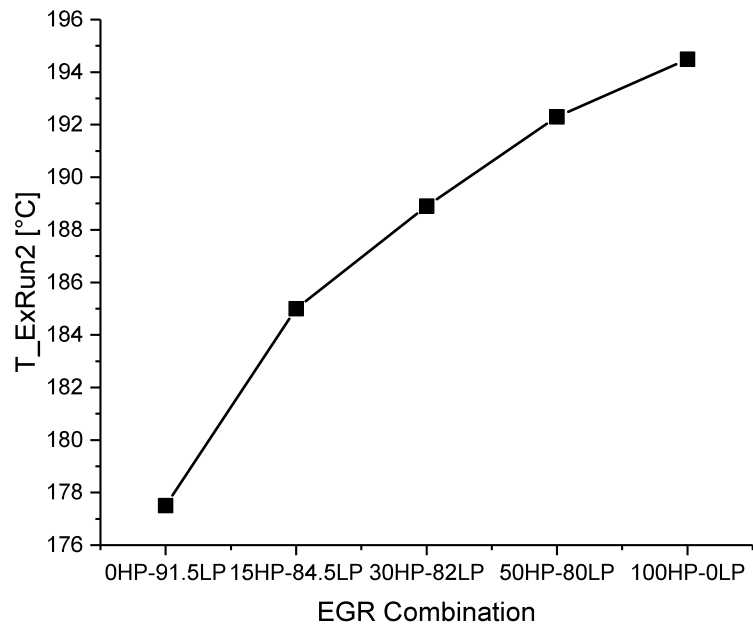


Figure 4.31: Temperature after HP EGR cooler for different HP-LP combinations.  $\lambda = 2.67 \pm 0.015$

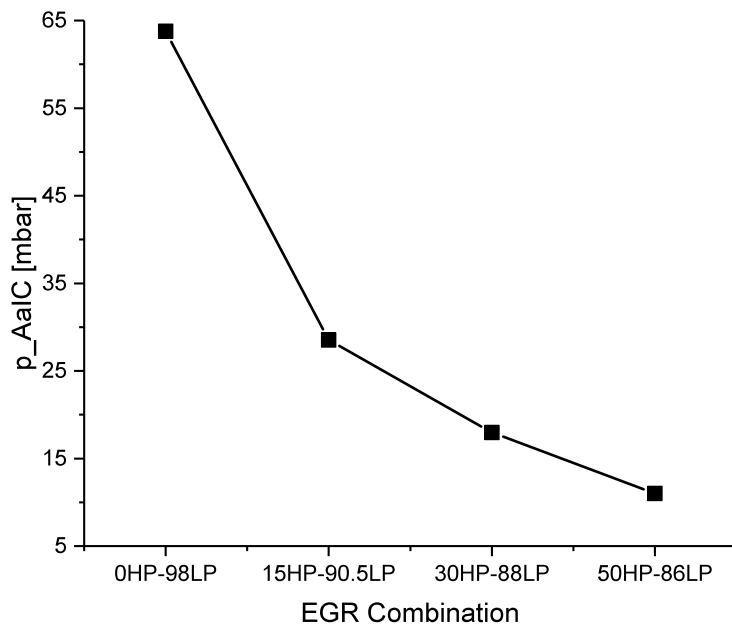


Figure 4.32: Air pressure after Inter-cooler for different HP-LP combinations.  $\lambda = 2.10 \pm 0.015$

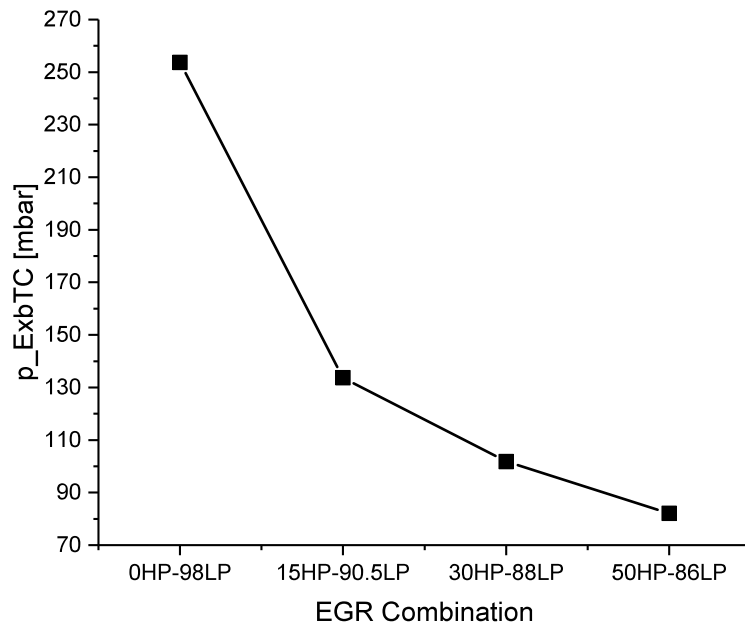


Figure 4.33: Exhaust pressure before turbocompressor for different HP-LP combinations.  $\lambda = 2.10 \pm 0.015$

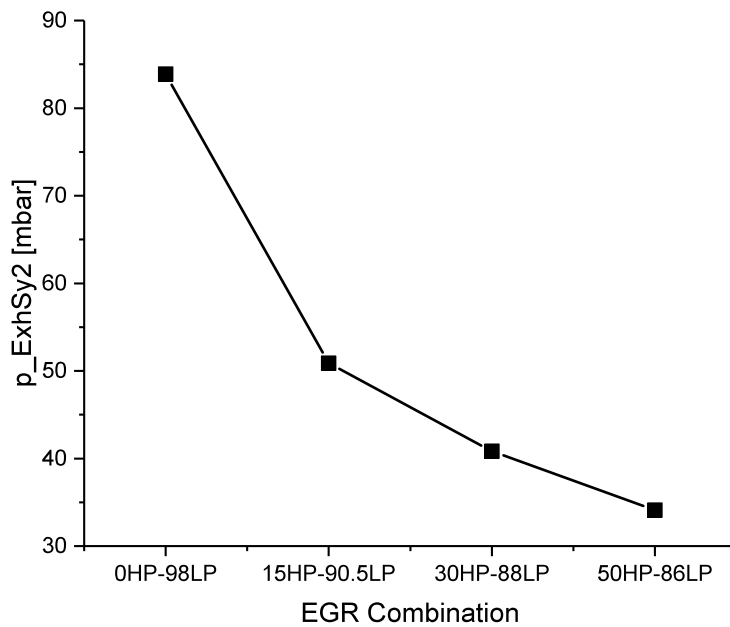


Figure 4.34: Pressure after HP EGR cooler for different HP-LP combinations.  $\lambda = 2.10 \pm 0.015$

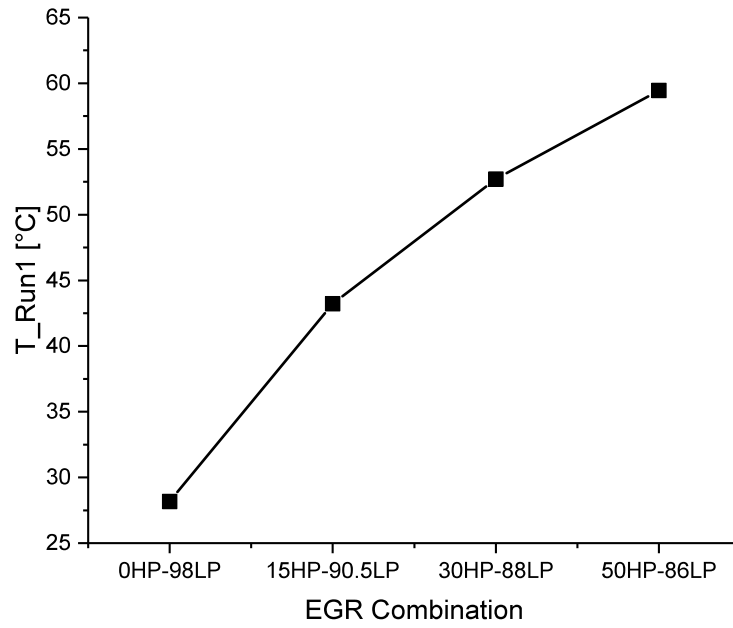


Figure 4.35: Temperature inside the intake manifold for different HP-LP combinations.  $\lambda = 2.10 \pm 0.015$

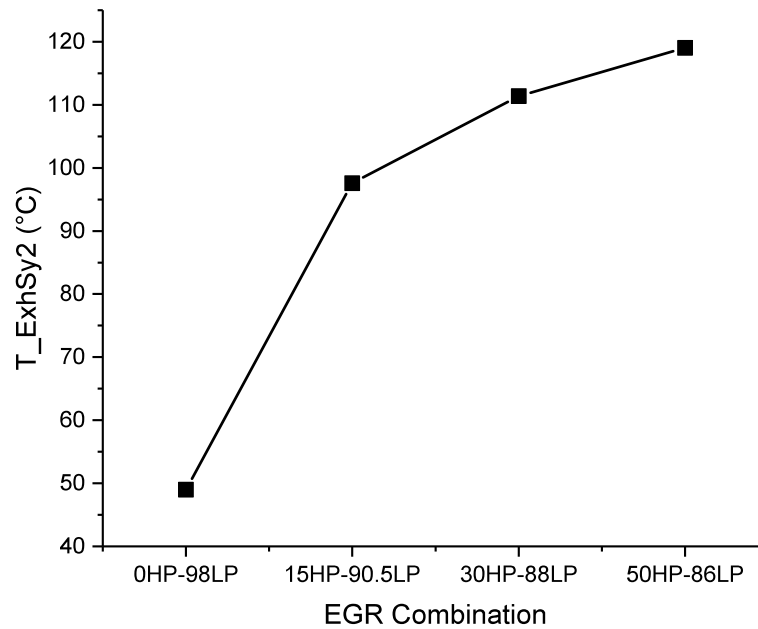


Figure 4.36: Temperature after HP EGR cooler for different HP-LP combinations.  $\lambda = 2.10 \pm 0.015$

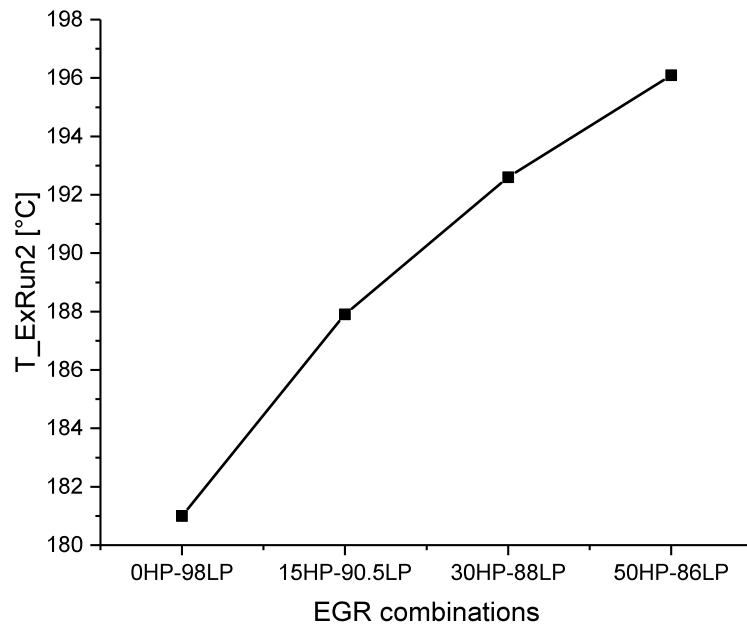


Figure 4.37: Temperature after HP EGR cooler for different HP-LP combinations.  
 $\lambda = 2.10 \pm 0.015$

# Chapter 5

## Future developments

Future experimental activity will cover a wide research area. The starting step will be the investigation of some engine operating points, chosen along with ENI and FPT. The procedure for the definition of tests will be briefly explained in the following sections.

### 5.1 Test plan

The first set of points is collected in Tab.5.2. The last point was chosen to investigate the medium-high load region in the engine map. It was computed starting from the power needed for motion of a vehicle running straight at a constant speed whose technical features are collected in Tab. 5.1.

Table 5.1: Vehicle dataset.

Variable	Unit	Value
V	<i>km/h</i>	122
S	<i>m<sup>2</sup></i>	5.658
<i>C<sub>x</sub></i>	-	0.35
m	<i>kg</i>	3500
<i>f<sub>0</sub></i>	-	0.01
<i>η<sub>t</sub></i>	-	0.95
<i>τ<sub>g</sub></i>	-	0.585
<i>τ<sub>f</sub></i>	-	4.22
Tires	-	215/75 R16
<i>V<sub>disp</sub></i>	<i>dm<sup>3</sup></i>	2.3

Table 5.2: Test plan.

Test number	Speed	Load
-	rpm	bar
1	1500	2
2	1500	8
3	2000	5
4	2500	2
5	2500	8
6	2192	14.5

The steps for its calculation are the following:

- Power needed for motion

$$P_n = RV = (R_r + R_a) V = mgf_0V + \frac{1}{2}\rho SC_x V^3 = 57.9 [kW] \quad (5.1)$$

- Engine power

$$P_e = \frac{P_n}{\eta_t} = 60.9 [kW] \quad (5.2)$$

- Engine speed

$$\omega_e = 2192 [rpm] \quad (5.3)$$

- Torque

$$T = 265 [Nm] \quad (5.4)$$

- bmep

$$bmep = 14.5 [bar] \quad (5.5)$$

The second set of points are those prescribed by the World Harmonized Steady State Cycle (WHSC). This new cycle replaced the older European Stationary Cycle (ESC) in Europe for testing heavy-duty engines starting from EURO VI standard. It was developed by the United Nations Economic Commission for Europe (UNECE) in order to aid the uniformity of all the regulatory legislation on pollutant emissions.

WHSC is a hot start ramped steady state cycle made up of 13 modes in which engine load and speed are precisely defined as percentages or normalized values (Tab.5.3). Therefore, global technical regulation (GTR) developed by the UNECE provides a denormalization procedure to compute the actual speed and torque values of the engine under-test. The speed is obtained as follows:

$$Actual\ speed = n_{norm} \cdot (0.45 \cdot n_{lo} + 0.45 \cdot n_{pref} + 0.1 \cdot n_{hi} + n_{idle}) \cdot 2.0327 + n_{idle} \quad (5.6)$$

where

- $n_{norm}$  is the percent speed in the second column of Tab.5.3.
- $n_{lo}$  «is the lowest speed where the power is 55% of maximum power»[22, p. 29] (Fig.5.1).

- $n_{pref}$  «is the engine speed where the maximum torque integral is 51% of the whole integral computed from  $n_{idle}$  to  $n_{95h}$ »[22, p. 29], as it is shown in Fig.5.2. « $n_{95h}$  is the highest speed where the power is 95% of maximum power»[22, p. 30] (Fig.5.1).
- $n_{hi}$  «is the highest speed where the power is 70% of maximum power»[22, p. 29].
- $n_{idle}$  is the idle speed (Fig.5.1).

Finally, the torque is computed

$$Actual\ torque = \frac{percent\ torque \cdot torque_{max}}{100} \quad (5.7)$$

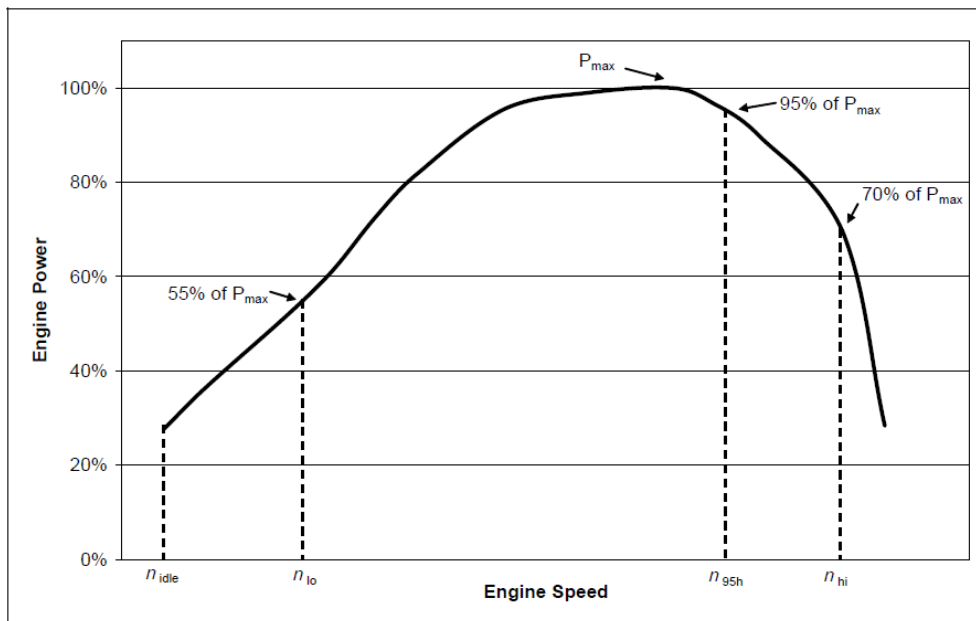


Figure 5.1: Definition of test speeds[22].

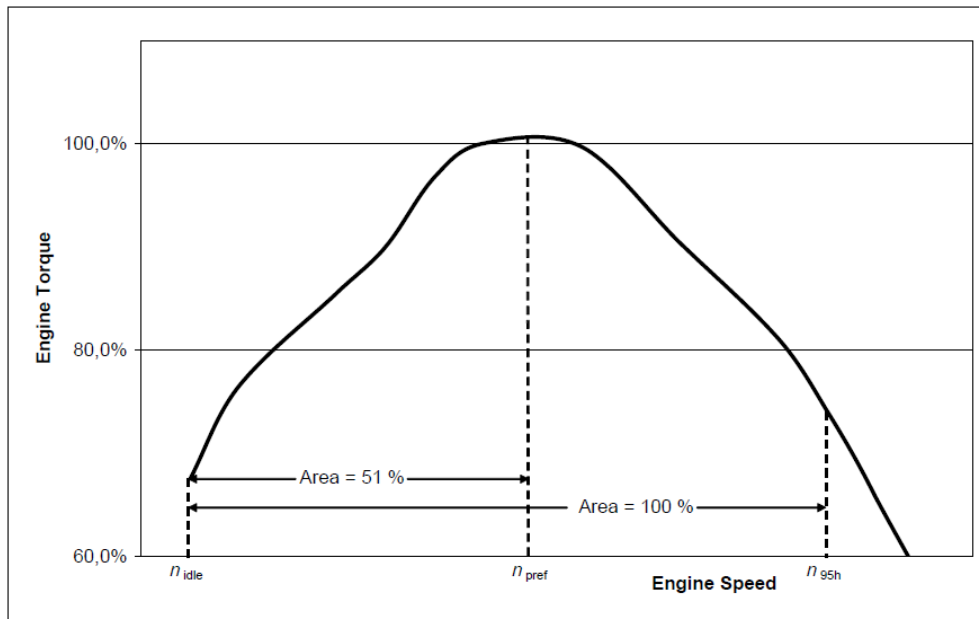


Figure 5.2: Definition of test reference speed[22].

Table 5.3: WHSC[22].

Mode	Speed	Load	Weighting Factor	Mode Length†
-	%	%	-	s
0	Motoring	-	0.24	-
1	0	0	0.17/2	210
2	55	100	0.02	50
3	55	25	0.1	250
4	55	70	0.03	75
5	35	100	0.02	50
6	25	25	0.08	200
7	45	70	0.03	75
8	45	25	0.06	150
9	55	50	0.05	125
10	75	100	0.02	50
11	35	50	0.08	200
12	35	25	0.1	250
13	0	0	0.17/2	210

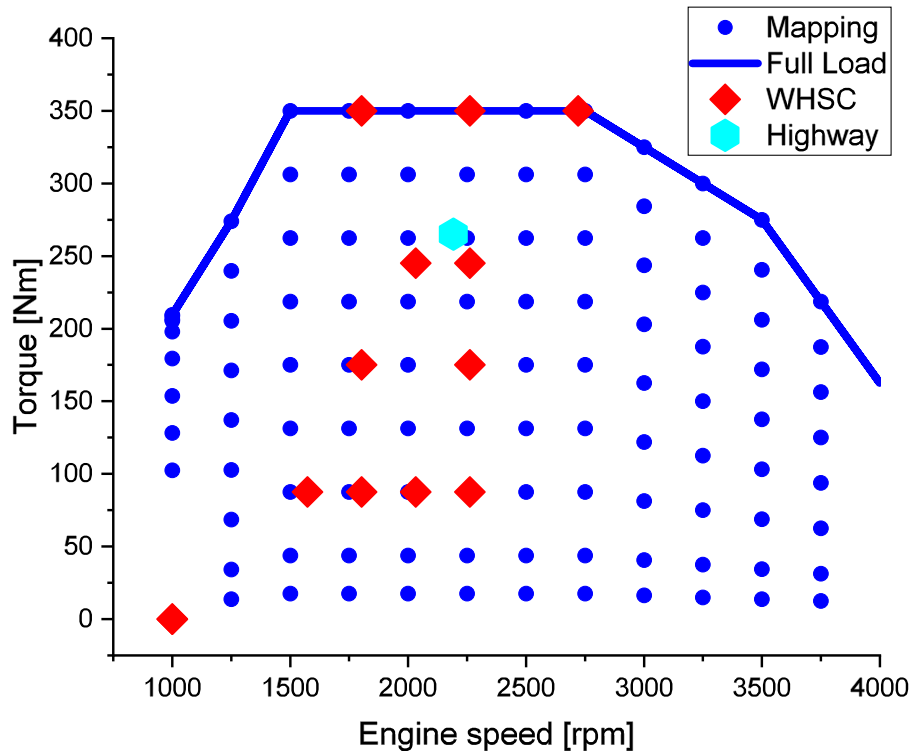


Figure 5.3: Engine map.

## 5.2 Alternative fuels

Another research activity that will be carried out in the future will concern the use of alternative fuels such as biodiesel (FAME, Fatty Acid Methyl Ester) and Hydrotreated Vegetable Oil (HVO). These fuels are spreading in automotive applications since they allow a significant reduction of Green House Gases (GHG) emissions.

Biodiesels are generally characterized by higher cetane numbers and better lubricating properties than conventional diesel fuels[3]. The main issues when using them are related to the higher boiling point and viscosity: the former can lead to dilution of the lubricating oil, with negative repercussions on the engine durability as well as ATS functioning, while the latter is a primary concern of the injection system[9]. Therefore, in order to limit the impact on the engine, biodiesel is typically blended with diesel fuels. The one that will be used in ICEAL is known as B7, and it is essentially a diesel fuel with a biodiesel content of 6.4%(V/V).

HVO is known as renewable diesel fuel. «HVOs are straight chain paraffinic hydrocarbons that are free of aromatics, oxygen, and sulfur and have high cetane numbers»[23, p. 1]. Unlike biodiesels, they do not show detrimental effects on the engine system, and they can also be handled more easily.

Table 5.4: Technical characteristics of HVO and B7 fuels.

	Unit	HVO	B7
Cetane number		75.5	53.9
Flashpoint	$^{\circ}C$	70	69
Viscosity at 40 $^{\circ}C$	$mm^2/s$	2.869	2.762
Distillation range			
60%(V/V) recovered	$^{\circ}C$	280.7	282
80%(V/V) recovered	$^{\circ}C$	286.1	310
recovered at 250 $^{\circ}C$	$\%(V/V)$	7.2	34.2
Total aromatics	$\%(m/m)$	<1.0	20.9
Polyaromatics	$\%(m/m)$	<0.1	2.8
Sulfur content	$mg/kg$	<3.0	5.4
Lubricity HFRR at 60 $^{\circ}C$	$\mu m$	316	214



# Chapter 6

## Conclusions

This thesis describes the installation on the test bench of a light-duty diesel engine for commercial vehicles. FPT Industrial provided the F1A engine that was adapted to the facilities in Politecnico through machining processes. The testing equipment, such as measuring sensors and exhaust analyzers, was mounted afterward.

The installation was complicated by several issues, which caused a lengthening of the time needed to complete this phase. As a consequence, it was possible to run a limited number of tests focusing mainly on the analysis of the EGR system functioning and its impact on the engine. The final part of this activity dealt with the preliminary investigation of the Dual Loop EGR system to be used as a starting point for future and more advanced studies.

The Dual Loop EGR system is made up of two independent circuits and then its complexity is increased significantly. It requires more advanced calibration and optimization strategies in order to control the two circuits simultaneously. For these reasons, during this activity it was not possible to fully investigate the DL EGR because of stability problems. Despite the complexity, the DL EGR allows improving the trade-off between the pollutant species. The LP EGR, in combination with the HP EGR, lowers the temperature of the intake charge, causing a reduction of the engine-out NO<sub>x</sub> emissions. Furthermore, it impacts on the combustion process by increasing the ignition delay that should be beneficial also in terms of soot reduction, even if this last effect could not be proved experimentally due to the malfunctioning of measuring instruments. Finally, the emissions of both CO and HC are raised, and they represent the main disadvantage of this system in the

analyzed conditions.

# Appendix A

## List of sensors

PoliTO name	pos.	Sensor type	Measure range	Accuracy	Description	FEM
PMAN1	1	Kistler 4007C005FDS1 - 2.0	0 - 5 [bar] A	≤1%FS	Intake manifold HF pressure	INDICOM 5
p_MAP	2	Druck PTX 611 PN PTX Ex-0129	-1 - 4 [bar] G 4 - 20 [mA]	±0.08%FS	Intake manifold LF pressure	6x1
PCYL1	3	Kistler 6058A42 SN 4547359	0 - 250 [bar] G	≤0.3 %FS	Cylinder 1 pressure	channel 1
PCYL2	4	Kistler 6058A42 SN 4547360	0 - 250 [bar] G	≤0.3 %FS	Cylinder 2 pressure	channel 2
PCYL3	5	Kistler 6058A42 SN 4547361	0 - 250 [bar] G	≤0.3 %FS	Cylinder 3 pressure	channel 3
PCYL4	6	Kistler 6058A42 SN 4547362	0 - 250 [bar] G	≤0.3 %FS	Cylinder 4 pressure	channel 4
PEXH1	7	Kistler 4049B10DS1 - 2.0 SN 4676631	0 - 10 [bar] A	≤0.3 %FS	Exhaust manifold HF pressure	channel 6
T_ExRun1	8	Thermocouple type KΦ3	0 / 1100 °C	Classe 1 ±0.004x t	Cylinder 1 exhaust temperature	10x5
T_EXRun2	9	Thermocouple type KΦ3	0 / 1100 °C	Classe 1 ±0.004x t	Cylinder 2 exhaust temperature	10x6
T_ExbTC	10	Thermocouple type KΦ3	0 / 1100 °C	Classe 1 ±0.004x t	Cylinder 3 exhaust temperature and before turbine	10x6
T_ExRun4	11	Thermocouple type KΦ3	0 / 1100 °C	Classe 1 ±0.004x t	Cylinder 4 exhaust temperature	10x8
T_Run1	12	Thermocouple type TΦ3	-185 / +300 °C	Classe 1 ±0.5°C	Cylinder 1 intake temperature and intake manifold temperature	10x1
p_ExbTC	16	Druck PTX611 PN PTX Ex-0129	0- 5 [bar] G 4 - 20 [mA]	±0.08%FS	Exhaust pressure before TC	6x15
Intake Emissions	17				Sampling point for intake gas	AMA
p_ExaTC (p sensor M)	18	Druck UNIK 5000 PN X5072-TB-A1-CA-HI-PA SN 3839371	-1 - 1.6 [bar] G 4 - 20 [mA]	±0.2%FS	Exhaust pressure after turbine	6x16
T_ExaTC	19	Thermocouple type KΦ3	0 / 1100 °C	Classe 1 ±0.004x t	Exhaust temperature after turbine	10x12
Engine-out emissions	20				Sampling point for exh. Emissions	AMA
p_AbIC (p2 (Abs))	21	MEAS U5200 PN U5341-000002-005BA	0- 5 [bar] A 1 - 5 [V]	±0.1%FS	Air pressure before intercooler	6x2
T_AbIC	22	PT100	-50 / +500 °C		Air temperature before intercooler	6x9
T_ExhSy1	23	Thermocouple type KΦ3	0 / 1100 °C	Classe 1 ±0.004x t	Exh. Temperature downstream EGR vlv	10x9
p_ExhSy1	13	Druck UNIK 5000 PN X5072-TB-A1-CA-HI-PA	0 - 6 [bar] G 4 - 20 [mA]	±0.2%FS	Exhaust p downstream EGR vlv	7x15

Table A.1: List of sensors of the experimental setup.

Polito name	pos.	Sensor type	Measure range	Accuracy	Description	FEM
T_ExhSy2	24	Thermocouple type KΦ3	0 / 1100 °C	Classe 1 ±0.004x t	Exhaust T downstream EGR cooler	10x10
p_ExhSy2	25	DSPM Industrie M210B-4B-G1/4-4-D2-P1-0.25%-S	0-4 [bar] G 4-20 [mA]	±0.25%FS	Exhaust p downstream EGR cooler	6x14
p_AaIC (p3 (Abs))	26	MEAS U5200	0-5 [bar] A	±0.1%FS	Air pressure after intercooler	6x3
T_AaIC	27	PN U5341-000002-005BA PT100	1-5 [V] -50 / +500 °C	±0.1%FS	Air temperature after intercooler	6x10
p_CWCin (p16 (Abs))	28	MEAS U5200 PN U5341-000002-005BA SN 8-062507F027	0-5 [bar] A 1-5 [V]	±0.1%FS	Coolant pressure engine-in	6x4
T_CWCin	29	PT100			Coolant temperature engine-in	6x11
p_CWCout (p17 (Abs))	30	MEAS U5200 PN U5341-000002-005BA SN 8-010911F078	0-5 [bar] A 1-5 [V]	±0.1%FS	Coolant pressure engine-out	6x5
T_CWCout	31	PT100	-50 / +500 °C		Coolant temperature engine-out	6x12
p_AbTC1 (p sensor P)	36	Druck UNIK 5000 PN X5072-TB-A1-CA-HI-PA SN 3803645	-1-1,6 [bar] G 4-20 [mA]	±0.2%FS	Air pressure before TC	7x3
T_AbTC1	37	Thermocouple type TΦ3	-185 / +300 °C	Classe 1 ±0.5°C	Air temperature before TC	10x15
p_Cabin	41	p_BARO	0,8-1,2 [bar] A 4-20 [mA] 0/50°C		Test cell ambient pressure	7x4
T_Cabin	42		0-10 [V]		Test cell ambient temperature	7x7
p_CcBbY1	43	Druck UNIK 5000 PTX PN X5072-TB-A1-CA-HI-PA SN 3843323	0-5 [bar] A	±0.2%FS	Fuel supply pressure	6x13
p_FuSup (p18 (Abs) )	44	Druck UNIK 5000 PTX PN PTX5012 SN 3931545	0-10 [bar] G 4-20 [mA]	±0.2%FS	Fuel supply pressure	6x6
p_FuRet	45	MEAS U5200 PN U5341-000002-005BA	0-5 [bar] A 1-5 [V]	±0.1%FS	Fuel backflow pressure	6x7
INJI	46	Tecktronix TCP305+TCA			Injector current signal	channel 7
T_OilGal	47	Thermocouple type K 3	0 / 1100 °C	Classe 1 ±0.004x t	Oil temperature at oil gallery	7x16
sBLBY	48	FEV BMR 75 0-10V			Volumetric flow rate through the blowby	7x12

Table A.2: List of sensors of the experimental setup.

PolifTo name	pos.	Sensor type	Measure range	Accuracy	Description	FEM
FlowCegr	50	Yokogawa AXFΦ32 SN S5R305311	0-2500 [l/h] 4-20 [mA]	±0.35%FS	EGR coolant flow rate (HP + LP) + EGR valve cooling	7x9
FlowCW	51	Yokogawa AXFΦ15 SN DIR301241	0-12000 [l/h] 4-20 [mA]	±0.35%FS	Coolant flow rate	7x8
P_oilGal (P sensor Q)	55	Druck UNIK 5000 PTX PN X5072-TB-A1-CA-H1-PA SN 3978037	0-10 [bar] G 4- 20 [mA]	±0.2%FS	Oil pressure at oil gallery	6x8
T_AirSno	58	PT100	0-50 °C 0– 10 [V]	Da modulo di conversione	Air temperature at the snorkle outlet	7x13
TExKist	62				Exh. Temperature kist sensor	10x11
ES636_Lambda	63				Lambda sensor to ES636	ES636 Channel 1

Table A.3: List of sensors of the experimental setup.

# Bibliography

- [1] Dec J.E. *A Conceptual Model of DI Diesel Combustion Based on Laser-sheet Imaging*. SAE International, 1997.
- [2] Flynn P. F. et al. *Diesel Combustion: An Integrated View Combining Laser Diagnostics, Chemical Kinetics, And Empirical Validation*. SAE International, 1999.
- [3] Heywood J. B. *Internal combustion engine fundamentals*. eng. 2nd ed. New York: McGraw-Hill, 2018.
- [4] Stiesch G. *Modeling Engine Spray and Combustion Processes*. Heat and Mass Transfer. Springer Berlin Heidelberg, 2013.
- [5] G. Ferrari. *Motori a combustione interna*. Esculapio, 2016.
- [6] Speight J.G. *Handbook of Petroleum Product Analysis*. Chemical Analysis: A Series of Monographs on Analytical Chemistry and Its Applications. Wiley, 2015.
- [7] Ferguson C.R. and Kirkpatrick A.T. *Internal Combustion Engines: Applied Thermosciences*. Wiley, 2015.
- [8] *BS EN 590:2013+A1:2017. Automotive fuels - Diesel - Requirements and test methods*. BS EN. 2013.
- [9] Reif K. *Diesel Engine Management: Systems and Components*. Bosch Professional Automotive Information. Springer Fachmedien Wiesbaden, 2014.
- [10] Merker G.P., Schwarz C., and Teichmann R. *Combustion Engines Development: Mixture Formation, Combustion, Emissions and Simulation*. Springer Berlin Heidelberg, 2011.

- [11] *BS ISO 8178-3:2019. Reciprocating internal combustion engines - Exhaust emission measurement.* BS ISO. 2019.
- [12] Millo F., Giacominetto P. F., and Bernardi M. G. “Analysis of different exhaust gas recirculation architectures for passenger car Diesel engines”. In: *Applied Energy* 98 (2012), pp. 79 –91.
- [13] Martyr A.J. and Plint M.A. *Engine Testing: Theory and Practice.* Elsevier Science, 2011.
- [15] Solinas A. “Installazione al banco, problematiche e messa a punto di un motore diesel heavy-duty Euro VI”. Politecnico di Torino.
- [16] Crovetto P. S. *Electric Systems in Vehicles.* 2018.
- [18] Wu J. *A Basic Guide to Thermocouple Measurements.* Texas Instruments, 2018.
- [19] Paulweber M. and Lebert K. *Powertrain Instrumentation and Test Systems: Development – Hybridization – Electrification.* Powertrain. Springer International Publishing, 2016.
- [20] Adachi M. and Nakamura H. *Engine Emissions Measurement Handbook.* SAE International, 2014.
- [21] *BS ISO 11614:1999. Reciprocating internal combustion compression-ignition engines - Apparatus for measurement of the opacity and for determination of the light absorption coefficient of exhaust gas.* BS ISO. 1999.
- [22] *Agreement on Global Technical Regulations (GTRs). Test procedure for compression-ignition (C.I.) engines and positive ignition (P.I.) engines fuelled with natural gas (NG) or liquefied petroleum gas (LPG) with regard to the emission of pollutants.* ECE TRANS 180 Add.4. 2007.
- [23] H. Aatola et al. “Hydrotreated Vegetable Oil (HVO) as a Renewable Diesel Fuel: Trade-off between NOx, Particulate Emission, and Fuel Consumption of a Heavy Duty Engine”. In: (2008).

# Sitography

- [14] *AVL documentation*. URL: <https://www.avl.com/measure-control>.
- [17] *Kistler documentation*. URL: [https://www.kistler.com/en/products/components/pressure-sensors/?pfv\\_metrics=metric](https://www.kistler.com/en/products/components/pressure-sensors/?pfv_metrics=metric).